2018

# Towards an in vitro innervated model of the cornea

Gilles Sebastiaan van Tienderen
*University of Wollongong*

UNIVERSITY
OF WOLLONGONG
AUSTRALIA

# Towards an *in vitro* innervated model of the cornea

Gilles Sebastiaan van Tienderen

Supervisors:
Gordon G Wallace,
Xiao Liu,
Stephen Beirne

This thesis is presented as part of the requirement for the conferral of the degree:

Master of Philosophy (M.Phil)

The University of Wollongong
Australian Institute of Innovative Materials (AIIM)
Intelligent Polymer Research Institute (IPRI)

July 2018

# Table of Contents

# Layman's summary

The cornea is a delicate structure found in the outermost layer of the eye. It is transparent, dome-shaped and plays a critical role in being able to see correctly. Each year, the economic burden of eye diseases and vision loss is estimated to be 139 billion dollars in the US. Furthermore, the market size of eye-related pharmaceuticals was approximately 12 billion dollars in 2010 in the US alone. However, despite these astounding numbers, developing new drugs for eye diseases has been difficult, with few drugs being developed each year. There are a lot of different factors influencing this disparity between money spent and drugs developed, one of them being a lack of understanding of the functioning of the cornea in its healthy and diseased state. Although the cornea is transparent and might seem to lack structure, it is a highly organized and complex tissue. In particular, innervation, i.e. the supply of nerves to the cornea, is critical for its function.

Biological models can be used to study the cornea and discover potential new drug targets. Currently, the most popular way to evaluate drug toxicity is through a 'Draize' test. In this test a substance is applied to the eye of a live rabbit, and the other eye is used as a control to see the difference. However, ethical concerns with using live animals, lack of reproducibility and the interspecies difference between humans and rabbits show that this test is not optimal. Development of *in vitro*, meaning in a controllable environment that's outside a living organism, 3-dimensional models can avoid these limitations.

Herein, we describe a novel 3D *in vitro* model for the cornea. We use novel fabrication techniques to modify common biomaterials to create a corneal model that includes innervation. We found that applying an electric current to collagen results in an optimal material for mimicking the cornea in a model. Additionally, we 3D printed live neuronal cells within another biomaterial and showed their survival. To guide the direction of the growth of neuron-like cells we fabricated very microparticles with neural growth factor inside. These were combined with collagen and the 3D printed neuron-like cells to create an overall model for the cornea with innervation. The current model requires further optimizing in regards to increasing innervation, although the first steps to producing a novel model have been taken.

# Abstract

Visual impairment due to corneal disease is a global health concern with few FDA-approved pharmaceuticals being developed. In the cornea, the interactions between the various cell types present are essential for its functioning. In particular, innervation through sensory nerves is crucial for optimal functioning of this tissue. However, the mechanisms underlying these interactions are poorly understood, and representative 3D innervated *in vitro* cornea models could be used as systems to model the native situation.

Therefore, an innervated model of the cornea is proposed and initiated. Electrocompacted collagen constructs serve as a basis for mimicking the cornea, and its mechanical, optical, and degradative properties are shown to be favorable. Furthermore, three dimensional extrusion-based printing has been employed to print methacrylated gelatin, and this scaffold was shown to support neuronal cell survival (83.4% viability 1 day after printing). A sustained release of neural growth factor to induce differentiation was established through incorporation of growth-factor loaded microparticles within the electrocompacted collagen. Additionally, the bioactivity was confirmed through an *in vitro* PC12 cell assay. The two biomaterials have been interfaced to fabricate a model to guide neuronal innervation. The current model shows potential in mimicking the complex structure of the cornea, but some optimization is required for neurite outgrowth. In the future, a viable *in vitro* corneal model could be used to provide fundamental insight into the process of corneal innervation and corneal diseases, as well as pre-clinical toxicity testing of new ocular drugs.

# Acknowledgments

I wish to express my sincere gratitude to my co-supervisors Dr. Xiao Liu and Dr. Stephen Beirne for their assistance during the entire project. I specifically would like to thank Xiao for allowing me to, at times, work independently, while, at other times, keeping me on the right track through expert guidance. I would additionally like to extend my gratitude to my clinical mentor, Dr. Gerard Sutton, for the support and advice during the monthly updates. Lastly, I would like to thank Prof. Dr. Gordon Wallace and Prof. Dr. Jos Malda for the opportunity to work within ACES and IPRI through the exchange program set up via the Biofabrication master's degree.

Additionally, I also worked on a review paper "Advanced fabrication approaches to controlled delivery systems for epilepsy treatment", currently under review, the abstract of which is added at the end of this report as additional information. For this, I would like to thank my co-authors Marius Berthel, Dr. Zhilian Yue, and Dr. Mark Cook and my previously mentioned supervisors.

# Certification

*I, Gilles van Tienderen, declare that this thesis submitted in fulfilment of the requirements for the conferral of the degree Biofabrication, from the University of Wollongong, is wholly my own work unless otherwise referenced or acknowledged. This document has not been submitted for qualifications at any other academic institution.*

_____

***Gilles Sebastiaan van Tienderen***
*27-6-2018*

# List of Names or Abbreviations

3D - Three-dimensional

ECM - Extracellular matrix

NGF – Neural growth factor

BDNF – Brain-derived neurotrophic factor

NT-3 – neurotrophin-3

GDNF – Glial cell line-derived neurotrophic factor

ATP – Adenosine triphosphate

RGD – Arg-Gly-Asp

GelMA – gelatin methacrylate

EC – electrocompaction

ECC – electrocompacted collagen

ITO - Indium tin oxide

PBS – Phosphate-buffer saline

DMSO – Dimethyl sulfoxide

UV – Iltraviolet

EM – Expansion medium

DM – Differentiation medium

DMEM – Dulbecco's Modified Eagle Medium

PCL - Polycaprolactone

LAP - Lithium phenyl-2,4,6-trimethylbenzoylphosphinate

PLGA – poly(lactic-co-glycolic acid)

DAPI - 4′,6-diamidino-2-phenylindole

DCM - Dichloromethane

PVA – Poly(vinyl alcohol)

ELISA – Enzyme-linked immunosorbent assay

FITC-BSA – Fluorescein isothiocyanate labelled bovine serum albumin

SEM – Scanning electron microscopy

MP(s)- Microparticle(s)

# List of Tables, Figures and Illustrations

Figure 10: Microscopic analysis of printed and seeded 10% w/v GelMA scaffolds 1 day post printing. Printed scaffold (A), (B). Seeded scaffold (C), (D). scale bars = 200 um

Figure 11: Live/dead staining of PC12 cells bioprinted within 10% w/v GelMA 1 day post printing. Live (left), dead (middle), and merged (right). Calcein/PI was used to stain the live (green) and dead (red) cells, respectively. Scale bar = 200 um

Figure 12: The effect of printing and seeding PC12 cells on their metabolic activity for the duration of 7 days measured via PrestoBlue.

Figure 13: Beta-III tubulin staining of PC12 cells printed within 10% w/v GelMA after 12 days. Neurite outgrowth can be seen going along the printed scaffold. Beta-III Tubulin is displayed in red and DAPI staining is displayed in blue. Scale bars = 200 um

Figure 14: Representative fluorescent microscopy pictures of w/o/w PLGA microparticles in aqueous solution at low (left) and high (right) magnification showing the spherical morphology and successful encapsulation of FITC-BSA within the microparticles. Scale bars = 200 um

Figure 15: Size distribution by fraction of growth factor loaded PLGA microparticles sized using ImageJ software. 0.5% PVA, 10% PLGA (A). 1% PVA, 20% PLGA (B). 0.5% PVA, 20% PLGA (C). 1% PVA, 25% PLGA (D).

Figure 16: Release curve showing the absolute cumulative release of neural growth factor from the 0.5% PVA 20% PLGA microparticles over a period of 8 days. Growth factor release was quantified using ELISA through generating a standard curve (top left) and fitting the unknown data points after subtracting background absorbance. All measurements were taken in triplicate.

Figure 17: Optical microscopic pictures displayed the behavior of the PC12 cells after culturing with or without NGF:MPs and empty control microparticles for the duration of 9 days. Black arrows indicate morphological changes and neurite outgrowth. Black dots are microparticles present in the medium. Scale bars = 200 um

Figure 18: Representative scanning electron microscopy (SEM) images of electrocompacted collagen without microparticles (A), with 5 mg/mL microparticles (B) and 10 mg/mL microparticles (C, D). (E) shows the disruption of ECC due to microparticle incorporation. Scale bars as indicated.

Figure 19: Live/Dead stainings of PC12 cells within 10% w/v GelMA. (A) middle of scaffold after electrocompaction of collagen. (B) Top of scaffold after electrocompaction of collagen. (C) Scaffold after undergoing the procedure without applying current. (D) control scaffold. Calcein/PI was used to stain alive (green) and dead (red) cells, respectively. Scale bars = 200 um

Figure 20: Live/Dead staining's of PC12 cells within 10% w/v GelMA after optimizing the effect of printing on cell viability after 1 day (left) and 7 days (right). Scale bars = 200 um

Figure 21: Beta-III tubulin staining of PC12 cells within the interfaced innervated model. Cells outgrow few neurites when NGF is dispersed within the medium (A, B). No sign of neurite outgrowth present in the interfaced innervated model of ECC:MP with 10% w/v GelMA (C, D). Neurite outgrowth can be seen extensively when seeded on top of 10% w/v GelMA (E, F), or when cultured with NGF:MP:ECC (G, H) . Beta-III Tubulin is displayed in red and DAPI staining is displayed in blue. Scale bars = 200 um

Table 1: Average sizes of the microparticles produced with different concentrations of PVA and PLGA. All values are represented as mean with std. error of mean

# Chapter 1: Introduction

A high-quality model of the cornea can provide new knowledge and insight on corneal functioning, both in regards to physiology and pathology. To develop a viable in vitro model of the cornea, it is critical to have a thorough understanding of the native cornea and its function in its healthy and diseased state. In this first chapter we describe the anatomy and structure of the cornea, with a more in depth look at innervation. Current materials for corneal bioengineering are discussed with their potential for *in vitro* models. Novel advanced biofabrication techniques are introduced, after which the aims of this research project are described.

## 1.1 Corneal structure, anatomy and functioning

The cornea is the outermost part of the human eye and consists of three main distinct layers: the epithelium, stroma and endothelium (Fig. 1). These three layers are separated by two acellular interfaces called the Bowman's layer and Descement's membrane.[1] The cornea is a transparent, avascular, connective tissue and is responsible for about 60% of the eye's refractive power.[2] Furthermore, it serves an important function as a protective barrier, both mechanically and pathologically (against infections). The thickness of the human cornea is around 500-600 um in the center and 600-800 um in the periphery, with a vertical and horizontal diameter of approximately 11-13 mm.[3,4] The cornea consists primarily of collagen fibers and some smaller proteoglycans, predominantly keratin sulfate and glycosaminoglycan.[5]

The corneal epithelium is the layer of the cornea that is directly in contact with the external environment, and makes up around 10% of the total corneal thickness.[6] Its main component is about 4-5 layers of stratified epithelial cells, which are held together by tight junctions.[7] The primary functions of the epithelium, together with the tear film, are to serve as a barrier against pathogen invasion, prevent loss of fluid and permit coherent refraction of light that enters the cornea.[8,9,10] The epithelium of the cornea is one of the most abundantly innervated tissues in the body, with free sensory and nociceptive nerve endings spread all along the outer surface.[11]

The corneal stroma constitutes 85-90% of the corneal thickness and is built up from aligned layers of collagen fibrils, also termed lamellae, and keratocytes.[12] Keratocytes are interspersed between the lamellae and provide the extracellular matrix (ECM) components of the stroma.[13] The collagen fibrils mainly consist of type I, V and VI collagen, with some of the previously mentioned proteoglycans interspacing the lamellae to allow for transparency and regulation of corneal hydration.[5,14] These organized collagen bundles provide the cornea with proper mechanical support, the right biophysical properties for maintenance of transparency as well as biochemical cues for keratocyte cell signalling.[15–17] In the healthy native cornea, transmittance,

as a surrogate for transparency, thresholds are around 80% at 380nm and more than 90% between 500 nm and 1300 nm. [17] It is clear that for any *in vitro* model to be viable it is critical to closely mimic this unique structure present in the cornea.

The corneal endothelial layer is a monolayer of endothelial cells that covers the posterior corneal surface.[18] Under healthy circumstances, the corneal endothelial cells do not proliferate. Their main function is to provide a metabolic active $Na^+/K^+$ pump to maintain healthy hydration levels in the corneal stroma by moving ions around and thereby using osmosis for water removal.[19] Correct hydration levels have been shown to be a necessity for transparency of the cornea.[20]

## 1.2 Corneal innervation

Corneal innervation is a component of the cornea that is interwoven in the stromal and epithelial layers of the cornea and is vital to the functioning of the cornea as a whole. The cornea is the most peripherally innervated surface of the human body.[21] The innervation originates from the trigeminal ganglion cells, which branch to form the limbal plexus, which in turn gives rise to stromal nerve trunks that enter the periphery of the corneal stroma.[22,23] The nerves are directionally orientated parallel to the lamellae in the cornea and as they move more superficially, they branch into various smaller neurites.[24] The growth and guidance of these nerves during the development of the cornea is modulated by various growth factors. Nerve growth factor (NGF) has been uncovered as one of the most important growth factors for nerve survival and regeneration, as well as axonal outgrowth, branching and sprouting.[25] Other important factors include brain-derived neurotrophic factor (BDNF), neurotrophin-3 (NT-3) and glial cell line-derived neurotropic factor (GDNF).[26,27] The interplay between these various

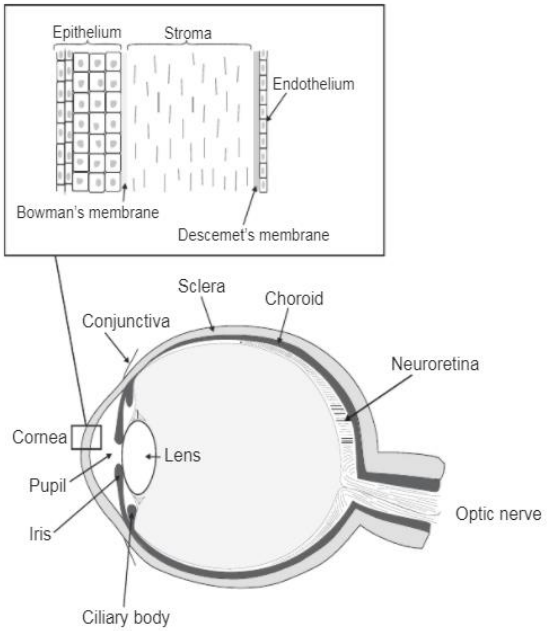


Figure 1: The anatomy of the cornea and eye. Adapted from Huhtala et al.[114]

growth factors forms the basis for the extensive innervation present in the cornea. Furthermore, mimicking the innervation as seen *in vivo* will rely on the ability of the corneal model to create a sustained release of NGF and/or other neuronal related growth factors.

The corneal nerves provide a platform for sensing, both mechanically and thermally, in order to maintain the overall health of the cornea. The particularly high density and unique exposure of the free nerve endings make the cornea (hyper)sensitive to noxious stimuli.[28] The nerves function by reaching the threshold of the receptors present, resulting in action potentials being relayed to the central nervous system. Among others, the innervation of the cornea plays an important role in wound healing and regeneration, the tear reflex and tear production and secretion.[29–31] These functions are regulated through a complex system of secretion and sensing of a multitude of neurotransmitters and peptides. A more extensive review on the various factors involved can be found in a recent review by Shaheen et al.[25] It has been established that the dysfunctioning of corneal nerves is frequently associated with corneal diseases, ultimately leading to a reduction in vision.[32] Despite this, the exact role of neuronal innervation, and the cellular mechanisms behind it, in the healthy and diseased state of the cornea are not fully elucidated.[33] This is partly due to the highly complex biochemical and anatomical pathways of corneal diseases that provide a hurdle for examination *in vivo*.[34,35] As a consequence, despite the relative high prevalence of corneal diseases, there are few therapeutic interventions available for corneal diseases.[25] More recently, research has delved into the use of a wide variety of biomaterials as building blocks for creating corneal tissue through bioengineering strategies.

## 1.3 Current cornea models

As may be evident, the primary functions of the cornea dictate important design considerations that a corneal tissue model will need to satisfy depending on the application. *In vitro* models can range from simple monolayered structures to full-thickness corneal substitutes. One of the earliest and simplest human models featured a layer of human primary epithelial cells cultured for toxicology testing.[36] More recent advances in human primary epithelial cells primarily focused on optimizing the *in vitro* culturing conditions with varying toxicity applications. For example, testing natural tear substitutes using cellular ATP as the parameter for defining toxicity showed potential therapeutic benefit of isotonic saliva and serum compared to pharmaceutical substitutes.[37] Various other mono-layered cultures of relevant corneal cell types have been published and some are currently commercially available.[38,39] Mostly, these rather elementary models may provide insight for immediate surface irritancy testing.[40] However, these models of the corneal epithelium layer do not accurately represent the multi-layered structure of the cornea as found *in vivo (fig. 2)*. Additionally, they lack all interactions between

different cell types present in the cornea. For applications focusing solely on the epithelial or endothelial component of the cornea, one can envision the lack of a supporting biomaterial not being crucial, as the *in vivo* situation mostly consists of a densely packed layer of cells. However, to mimic the stroma of the cornea, or a combination of multiple layers, it is of utmost importance to choose a suitable material as well as the correct cell source. A wide variety of materials have been studied with the goal of exploring fundamental research on cornea and finding alternatives for current corneal dysfunction treatments. Both natural and synthetic polymers have been studied, including silk, gelatin, chitosan, collagen and other synthetic polymers. As a complete overview of all usable materials is beyond the scope of this thesis, and has been done exhaustively by Chen et al.[41] , the focus will be primarily on certain characteristics that are needed to allow for optimal corneal tissue mimicking and the biomaterials that can provide these characteristics within the scope of *in vitro* models. To note, in principle, complex 3D tissue models should be proficient at mimicking the human cornea, compared to simple 2D cell culture models (fig. 3). However, so far the difference has not been apparent.[42] Surprisingly little research has been published on recapitulating the cornea in a 3D model. Thus, whether this phenomenon (2D =3D models in cornea) is due to the lack of research on 3D corneal models remains to be seen. The need for increased attention for reliable models is shown by the clinical need for these advanced models (see Box 1).

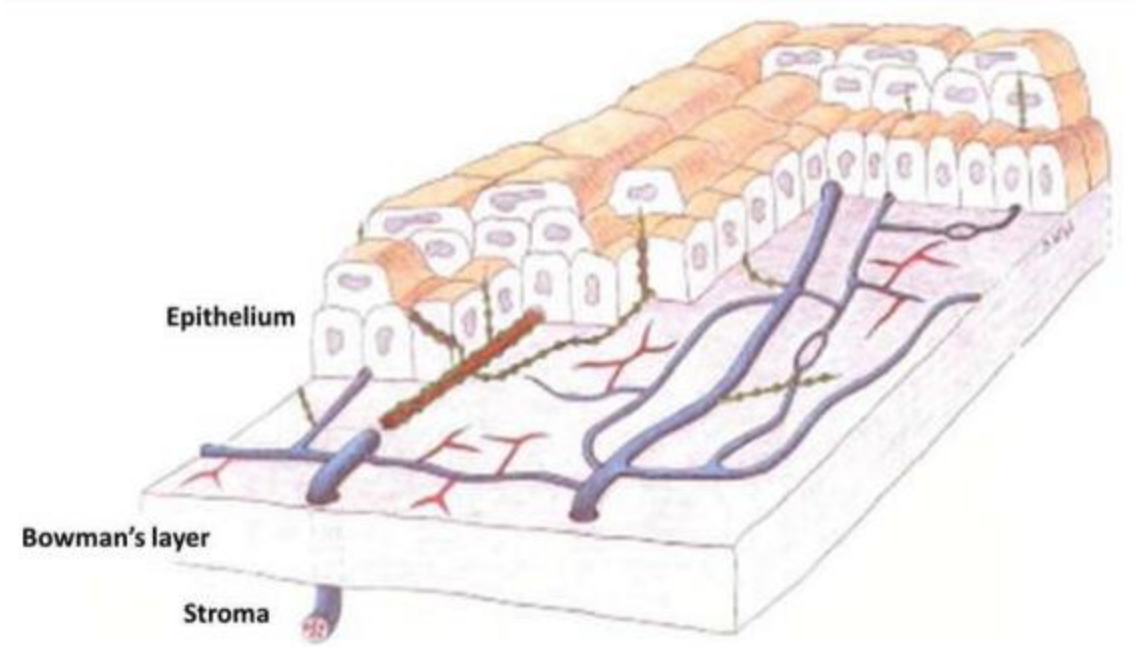


*Figure 2: A schematic depiction of the distribution of human nerves in the cornea. Unmyelinated nerves (blue) are made up out of straight (red) and beaded (green) fibers. Obtained from Muller et al.[113]*

**Box 1. Clinical need for *in vitro* cornea models**

The ophthalmic drugs market has been increasing in value continuously from 12 billion in 2010 to approximately 52.4 billion in 2017.[99] This has resulted in more investments from the large pharma companies such as Merck and Pfizer. Although the pharmaceutical market has been growing heavily, the amount of drugs approved by the FDA has decreased in recent years.[99] Although there are a variety of reasons contributing to this, an important factor remains the lack of fundamental understanding of corneal functioning together with difficulties in developing reliable pre-clinical testing methods.[100,101]

The current gold standard for evaluating drug toxicity is the *in vivo* Draize test performed on rabbit corneas.[102] In this test, the substance is applied to one eye of the rabbit, while the other eye is used as a control. Besides ethical concerns, there is a lack of reproducibility and the interspecies differences result in inconsistencies with human responses.[103,104] As an alternative, *ex vivo* cornea models have been developed by isolating animal corneas.[105,106] Nevertheless, these models share similar limitations to the Draize test. On top of that, the pain response cannot be established as the excision of the cornea results in irreparable nerve damage.[107] These limitations can be avoided by the development of new *in vitro* models. These models minimize ethical concerns, are more cost-effective, able to utilize human cells, and can provide higher throughput analysis for drug testing and screening.[108] Three-dimensional models have first been developed using a variety of animal cell sources, including bovine, mouse and pig.[109–111] Additionally, various *in vitro* models solely using (immortalized) human corneal cells have also been published.[40,57,112]

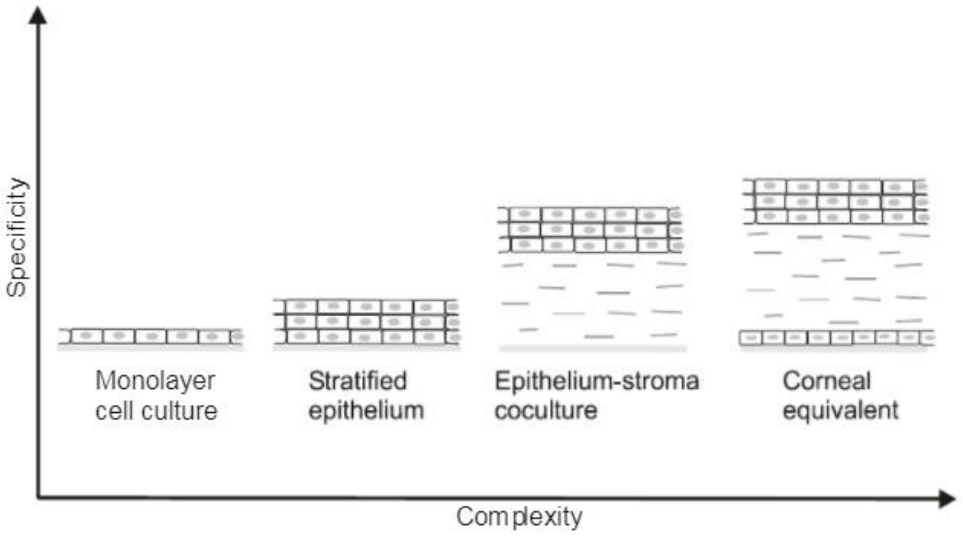


Figure 3: Development of cornea tissue models. Obtained from Huhtala et al.[49]

## 1.4 Biomaterials for corneal model fabrication

### 1.4.1 Gelatin

Gelatin is a natural polymer derived from the (partial) hydrolysis of collagen. Due to its biocompatibility, biodegradability and inexpensiveness it has been widely used in a range of tissue engineering strategies, including bone, skin and cornea. Gelatin has inherent cell binding motifs, most importantly Arg-Gly-Asp (RGD), allowing for relatively good cell adherence and spreading. This has been shown through the seeding of human endothelial corneal cells and precursor fibroblasts.[43,44] Due to its relatively close proximity in structure to collagen, gelatin is a potential biomaterial well-suited for corneal applications. However, modifications are usually required to give it proper structural fidelity.[45] Gelatin methacrylate (GelMA) is a popular gelatin derivative that is modified so that covalent cross-linking can occur through photo-initiated radical polymerization.[46] This semi-synthetic semi-natural material keeps the advantageous cell binding motifs of gelatin while obtaining the tunable physical characteristics usually only seen in synthetic materials. Its variability in chemical and mechanical properties due to the wide variety of crosslinkers that are compatible with gelatin shows potential for corneal *in vitro* models, however, similar mechanical properties to native cornea have not been achieved to this date.[47] GelMA has been widely used as a tunable scaffold for a variety of cell types, however little research has been done on combining it with corneal relevant cell types and, to our knowledge, no corneal 3D models have been fabricated using gelatin as a major component.

### 1.4.2 Silk

Silk is a naturally-sourced biomaterial that has been utilized as a substrate for corneal applications due to its natural optical clarity, mechanical robustness and tunable chemical modifications.[48] Unmodified silk membranes do not contain RGD motifs, and although they provide similar cell attachment properties as seen on plastic culture substrates, RGD-containing materials (i.e. gelatin) show increased cell responses. Coupling of a RGD motif to the silk film provided better cell attachment, as well as increased expression of collagen type I and IV, both abundant in native cornea.[49] An apparent advantage of silk over gelatin is the potential of patterning, which has been shown to be critical in the behavior of corneal cells.[50] For example, the topography of silk, depending on the depth and width of grooves introduced into the substrate, influenced the attachment, proliferation and migration of human corneal epithelial cells.[50,51] Additionally, modified silk films can obtain similar elastic moduli to the cornea, although these elastic moduli have only been shown by using water vapor annealing as a crosslinking method.[52] Interestingly, the combination of this crosslinking technique and biomaterial has not been further explored for corneal tissue engineering. Notably, the most recent development in a full-scale corneal equivalent model used silk as a basis for the culture

of human corneal stromal stem cells, human corneal epithelial cells and DRG neurons.[53] This is the first reported model that was able to successfully integrate all three cell types within a single model. Furthermore, an air-liquid interface was included to mimic the native corneal interface, and the addition of innervation showed an improvement in viability of both corneal cell types. Importantly, to guide neuronal innervation NGF was patterned within the silk film and loaded within the hydrogel. Although this corneal model is the most sophisticated model produced so far, some limitations have to be taken into consideration. The base biomaterial is mismatched with native cornea, and, more importantly, the unique structure of the cornea, with approx. 200 lamellae layered together to form a thickness of 500 um, is not represented well by the few layers of silk film used in this model. Lastly, the mechanical strength/elastic moduli of the construct is not reported.

### 1.4.3 Collagen

As mentioned previously, collagen is the most abundant protein in the human cornea and for that reason an ideal biomaterial for use in corneal tissue engineering. Collagen is available through a wide variety of sources, including animal-derived and recombinant, as well as from a variety of tissues (tail, skin, etc.). The source and tissue of origin of collagen can have a large effect on its properties and performance, hence choosing the right collagen to utilize is paramount to its success. Research has established the effect of particular sources of collagen on important characteristics (tensile strength, denaturation temperate, light transmittance and fibril alignment) that are of particular relevance for corneal applications.[54] Hydrogels based on collagen are biodegradable and biocompatible with a variety of corneal-related cell types, including limbal epithelial cells and primary stromal fibroblasts.[55,56] In regards to cellular response and interaction, collagen is a biomaterial that is best suited for corneal applications, without exception. However, unmodified collagen is compliant and has low mechanical stiffness, making it unsuited for corneal tissue engineering. Naturally, much of the research on collagen for corneal applications has been focused on modifying collagen, chemically or physically, to increase its mechanical performance. Crosslinking is a common method of increasing the strength of collagen hydrogels, primarily collagen type I. Crosslinking usually refers to the process of chemically joining two molecules through covalent bonding, commonly through cleaving and/or attaching chemical groups to the original substrate. It is important to take into consideration that with chemical crosslinking some agents have toxic effects (through e.g. the generation of toxic side-products) on cells, including a variety of corneal cell types. Thus, research has been focused on identifying cytocompatible cross-linking agents, such as riboflavin, genipin, and EDC-NHS.. [57] Interestingly, Duan et al. found that chemical crosslinking resulted in collagen hydrogels that not only had enhanced mechanical properties, but also increased optical transparency.[58] The most common agent used is EDC-NHS. This

method strengthens the hydrogel by crosslinking carboxylic acids with primary amines.[59] However, the strength and stiffness currently achieved with this agent was at least one order of magnitude lower than native cornea. Furthermore, it is important to note that although the transparency of the biomaterial did increase, the collagen fibers present had a lack of organization and direction, unlike the structural assembly of collagen fibers found in native cornea.[60]

A major discrepancy between collagen used *in vitro* and natural collagen containing tissues in the body is density of the collagen molecules because of their compaction. In the body collagen structures can be as dense as 250-400 mg/mL, while for hydrogels this is usually contained with the range of 1-10 mg/mL. Collagen is an ampholytic molecule by nature, which means that it can obtain different charges at different pH levels (-0.8 coulombs at pH of 3, +0.8 coulombs at pH 11).[61] These characteristics resulted in the development of an electrochemical compaction method for collagen.[61] Herein, the collagen molecules closely pack together at the isoelectric point, which is the point where the net charge of the collagen molecules is zero. Building on this, Kishore et al. showed the potential of electrocompacted collagen, with EDC-NHS crosslinking, as a basis for corneal applications (fig. 4).[62]

Collagen has been used previously for *in vitro* corneal model applications. Ahearne et al. used a basic collagen-based *in vitro* model of the cornea, specifically focusing on wound healing, to monitor the effect of collagen and cell concentration on cell-matrix interactions.[63] The relatively novel realization of the importance of corneal innervation, has led research to be focused on tissue models that include a neuronal aspect. Suuronen et al. used chicken-derived dorsal root ganglion (DRG) neurons to innervate a model containing corneal endothelium and stroma.[64] The neurons and corneal cells were cultured in a collagen hydrogel, and the addition of innervation resulted in an increased proliferation of the endothelial cells. Nevertheless, the density of nerve

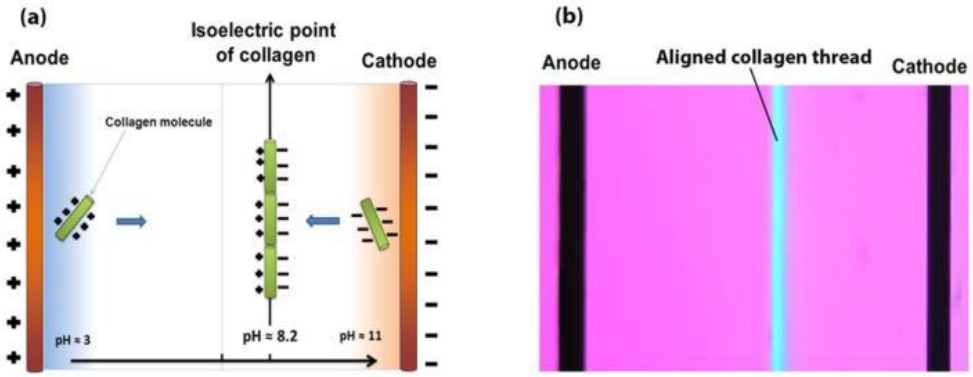


Figure 4: Mechanisms of electrocompaction of an aligned collagen thread. Adapted from Younesi et al.[77]

endings were significantly lower compared to native cornea, the collagen hydrogel had low mechanical stiffness and the epithelial layer was not included in the model. Another 3D corneal model, consisting of ND7/23 sensory neurons and a human corneal cell line interestingly showed that the incorporation of the neurons did not influence the barrier function of the corneal epithelial cells. Additionally, although not yet explored in relation to corneal models, PC12 cells have been used extensively as models for neuronal innervation and neurosecretion.[65,66] In all, the use of conventional collagen hydrogels in corneal tissue engineering has been highly prevalent, however the issue of mechanical properties is a recurring problem for these types of constructs.[67]

## 1.5 Biofabrication techniques for corneal applications

A particular field of interest for innovation within the scope of corneal tissue engineering is the convergence of cell biology and advanced fabrication methods, also referred to as biofabrication. One novel fabrication technique, the previously mentioned electrocompaction technique, provides a solution to address the problem of low mechanical stiffness.

### 1.5.1 3D Bioprinting

In the field of biofabrication, 3D bioprinting is a technique that has gained significant attention for tissue engineering applications due to its ability to create a hierarchical assembly of biological structures using 3D printing technology. Herein, optimal nutrient diffusion and spatio-temporal localization of cells can be achieved through deposition of bio-inks in a predefined pattern. A variety of 3D bioprinting techniques have been developed and investigated, although seldom for corneal applications.

Using laser-assisted bioprinting and corneal limbal stem cells Sorkio et al. were able to create a layered structure mimicking the stroma. In short, laser-assisted bioprinting uses a pulsed laser to produce a jet of solution which can be deposited onto a substrate.[68] With this technique, high resolution and high cell density prints can be produced. The stem cells were situated inside a bioink consisting of recombinant laminin and collagen type I, specifically adapted to the laser-based printing setup. Microstructure analysis, extensive protein expression analysis and cell viability results showed the potential of using laser-assisted bioprinting for corneal applications.[68] Very recently, Isaacson et al. used a 3D digital human corneal model to bioprint corneal keratocytes to create a biosynthetic corneal structure using extrusion-based 3D printing. This printing method employs a pneumatic-, mechanical- or solenoid-based system to deposit viscous and semi-liquid materials from a nozzle in a layer-by-layer fashion. The keratocytes were printed within a collagen/alginate bioink, and showed relatively high viability post printing. However, no other biological properties were investigated, such as differentiation or cell attachment properties. Furthermore, no *in vitro* characterization was done on the printed

structures (e.g. mechanical strength, transparency, stability, etc.). Lastly, the bioink had very low fidelity during the printing process, and a commercially available support structure was required to maintain shape and structure.[69] For neuronal innervation, similar to other cellular processes, it is important that nutrient diffusion is sufficient to sustain proliferation and differentiation of the cells. Additionally, while 2D neural cell cultures have their place in studying certain aspects of neural development, 3D cultures are able to more accurately represent the *in vivo* microenvironment of neural tissues.[114] Particularly, 3D bioprinting of neuronal constructs allows for defined control over the neuronal microenvironment, both through the bioink and potentially by addition of other (growth) factors to the bioink. The spatiotemporal patterning of the cells and growth factors allows for precise control over neuronal outgrowth, and thus can be used to better recapitulate the native environment.[115] To this regard, extrusion-based bioprinting could be used for corneal innervation applications.

All innervated corneal models previously described shared the characteristic of NGF-guided neurite extension, whether through stamped silk films, addition within a collagen hydrogel or otherwise. One avenue which has not been previously explored in relation to corneal models is the fabrication of microparticles. Growth factor-loaded microparticles have been used for a variety of sustained release applications, including *in vivo* intracerebral implantation and bone tissue regeneration.[70,71] This method of creating a relatively long-term release of neural growth factor could hold potential for applications within 3D *in vitro* corneal models.

All in all, 3D cornea *in vitro* models hold potential to complement currently employed models for a variety of applications, ranging from basic fundamental research to drug toxicity testing. However, the small volume of research currently published on these models show the need for further investigations. As it stands, the current generation of *in vitro* 3D corneal models lack one or more of these features:

(i) full representation of the multi-layered cornea structure, particularly stroma.

(ii) The incorporation and interaction of the different cell types present in the cornea (nerves/epithelial/endothelial/keratocytes).

(iii) A sustained function for a longer period of time (>7 days required for basic *in vitro* testing and sufficient neurite outgrowth)

(iv) similar mechanical properties to native cornea, wich have a Young's modulus of approx. 290 kPa. [80]

## 1.6 Aims

To address these issues, the ultimate aim is to create an *in vitro* 3D corneal tissue model that represents corneal tissue in regards to the distinctive layers present *in vivo*, containing multiple cell types and allowing for guidance of neurite outgrowth. For this project, the focus will be on creating a platform for neuronal survival and differentiation. The neuronal cell source utilized will be PC12 cells. For this reason, a sustained release of neural growth factor has to be achieved to create a guided innervation model. Additionally, an emphasis will be on investigating electrocompaction of collagen as a competent biomaterial to mimic the native cornea.

The specific aims of this project are:

(i) Investigate electrocompacted collagen as an optimal material for 3D *in vitro* corneal models,

(ii) Perform extrusion-based bioprinting with GelMA to provide a basis for neuronal cell survival,

(iii) Establish a method of sustained release of neural growth factor through fabrication of microparticles,

(iv) Create an innervated model of the cornea through interfacing (i), (ii), and (iii) in a single construct.

# Chapter 2: Materials and Methods

## 2.1 Electrocompacted Collagen production

### 2.1.1 Electrocompaction (EC) chamber fabrication

The EC chamber consists of three main components, a cathode, an anode and a spacer (see suppl. Fig. 1). The top part is ITO-coated glass (30x30 mm), cut to dimensions with a glass cutter. The ITO coating enables the glass to be conductive, thus acting as the cathode. The bottom part is a stainless steel plate (35x35 mm). The stainless steel is conductive and acts as the anode. A small copper strip is attached to both the ITO-coated glass and stainless steel plate to allow for crocodile clips to be attached. In the middle a non-conductive spacer is required to prevent short circuiting. The spacer is made out of standard acrylic, cut to custom dimensions with a laser cutter (Universal Laser Systems GmbH, Vienna, Austria). The height of the chamber can be adjusted by using multiple layers of acrylic. The complete set-up is held together with clamps to prevent leakage (suppl. fig. 1). The process of electrocompaction can take place due to the previously mentioned ampholytic nature of collagen (fig. 3).

### 2.1.2 Fabrication of EC collagen sheets

6 mg/ml Type-1 bovine collagen solution (Nutragen, Advanced BioMatrix, CA, USA) was diluted with sterile deionized $H_2O$ to 3 mg/ml. Afterwards, it was dialyzed against deionized water for 24-48h at 4°C, refreshing the water a total of 4-6 times. After dialysis the collagen solution is injected into the EC chamber via a 1 mL syringe and needle. By using the ITO-coated glass as an anode and the stainless steel plate as a cathode a constant voltage (5v, 600 s, e^-003 sensitivity) is applied to the collagen solution through the use of an electrochemical workstation (CH Instruments, Texas, USA). The electric current results in a formation of a pH gradient which, due to the amphoteric nature of collagen, causes the collagen molecules to migrate and align close to the isoelectric point. After the electrocompaction process is completed the collagen sheet can be harvested from the anode. To promote fibril formation after the process of electrocompaction, the collagen sheet is incubated in 10x PBS at 37 °C for 3h.

### 2.1.3 Crosslinking of EC collagen sheets

To enhance the mechanical properties and stability of the EC collagen crosslinking occurred post-electrocompaction. 10 mM riboflavin was dissolved in 10 mL DMSO, after which it was added to 90 mL $H_2O$ and used as a crosslinking agent. After incubation in PBS the collagen sheets were transferred to the riboflavin solution and re-incubated for 4h at 37 °C. Hereafter, 365 nm UV-light with a 100 W lamp (90% intensity) was applied for 120s using a UV LED

curing system (Model no. S1000-1B, Lumen Dynamics, Mississauga, Canada). To remove the residual riboflavin crosslinking solution the collagen sheet was incubated in PBS for 5h. The final incubation in PBS allows the yellow color from the riboflavin solution to be removed from the collagen sheet.

### 2.1.4 Mechanical assessment

To assess the mechanical properties of ECC tensile testing was performed using a Shimadzu EZ mechanical tester with a 10N sensor attached. After calibration, tensile tests were performed on ECC with fixed dimensions (15 x 5 mm) (n = 3). In short, samples were attached to paper tabs to allow for clamping without destruction of the material. The thickness of the ECC was measured with a microscope and three values were taken and averaged. Uniaxial tensile loading was performed until failure with a strain rate of 1 mm/min. Load vs displacement data was used to determine the stress strain curves and in turn calculate the ultimate stress, ultimate strain, young's modulus and tensile modulus. Tensile strength is classically defined as the value of the maximum stress that a material can handle. Young's modulus is defined as the slope at the beginning of the curve . See Suppl. Fig. 2 for a graphical representation.

### 2.1.5 *In vitro* passive degradation assessment

To assess degradation of electrocompacted collagen *in vitro* an assay based on polymer dry weight was performed (n = 3). The electrocompacted collagen samples were prepared as described in 2.1.3 and 2.1.4. Next, the samples were incubated in culture medium with standard culture conditions. The constructs were frozen at -80 °C and subsequently freeze dried overnight using an ALPHA 2-4 LDplus (Martin Christ, Osterode am Harz, Germany). The dry weight of the sample was measured at D0, D4, D7 and D14. The degradation was determined through the equation:

$(WT_0 - WT_x)/ WT_0 \times 100$

Wherein x refers to the specific time point that the weight was measured at and W = dry weight. Thus, $WT_0$ is the weight pre-degradation and $WT_x$ the weight at timepoint x.

## 2.2 Bioprinting

### 2.2.1 Cell culture

Rat adrenal medulla PC12 cells were obtained from American Type Culture Collection (ATCC). PC12 cells were cultured in high-glucose Dulbecco's Modified Eagle's Medium (DMEM) (+L-glutamine, + sodium-pyruvate, + pyridoxine hydrochloride) (Life Technologies, California, USA), prepared according to manufacturer's instructions. The medium was

supplemented with 10% fetal bovine serum (Life Technologies), 5% horse serum (Life technologies) and 1% Penicillin/Streptomycin (Life Technologies) to produce culture medium (CM) conditions. PC12 cells were maintained at standard cell culture conditions (humidified 37C, 5% CO2) and passaged 1:4 every 7 days. To differentiate the cells the medium was changed to high-glucose DMEM supplemented with 1% horse serum (Life Technologies) and 5 ng/mL neural growth factor (NGF), hereafter referred to as differentiation medium (DM) (Invitrogen, California, USA).

### 2.2.2 3D printing of polycaprolactone (PCL)

PCL printing was facilitated by a modified BioBots printer (Allevi, Philadelphia, USA). The extrusion of PCL was pneumatically driven with a pressure of 0.113 MPa. 200 μm nozzle-tips were used for extruding at a temperature of 119 °C. To prevent the print from dislodging during the printing process the build plate was heated to approximately 30 °C. Velocity of the printing was 5 mm/s with a grid infill percentage of 15%. 10x10mm scaffolds of various heights ( ranging from 0.3 to 4 mm) were produced for incorporation of EC collagen. Methacrylated gelatin (GelMA) bioprinting was attempted with the modified BioBots printer, but failed to print reliable strands due to temperature variability within the system (n > 5 attempts). As a consequence, future GelMA printing was done with the 3D Bioplotter (EnvisionTEC, Gladbeck, Germany).

### 2.2.3 3D printing of GelMA

GelMA was mixed with its photo initiator, in this case LAP, at 0.05% v/v. Printing of GelMA constructs was attempted using 10% w/v GelMA. For live cell printing, the cells were incorporated into the bioink right before loading of the cartridge. Cells were incorporated at a concentration of $2.0 \times 10^6$ cells/mL. To print scaffolds with high fidelity the cartridge was heated up to 23 °C, while printing occurred at a pressure of 2.5 bar and 6 mm/s. Lastly, the base plate was cooled to 10 °C.

SolidWorks™ was used to produce cuboidal scaffolds of 10x10 mm as base architecture. The scaffolds were exported as .stl files and sliced using the RP software for the 3D Bioplotter at 120 um layer slicing. Infill percentages of the cuboids were set to 0° and 90° angles, with 1 mm distance, and four layers were printed in total. The printed GelMA scaffolds were subsequently crosslinked for 60 seconds with 365 nm UV-light with a 100 W lamp using a UV LED curing system (Model no. S1000-1B, Lumen Dynamics, Mississauga, Canada). For live cell printing, scaffolds containing cells were immediately placed into sterile petri dishes with 1 mL of culture medium and placed on a 37 °C plate (n = 6).

### 2.2.4 Transparency

In order to assess the transparency of the collagen and GelMA samples, light transmission measurements were performed using a UV-vis spectrophotometer (UV-1800, Shumadzu, Kyoto, Japan). Non-EC and EC collagen samples (n = 3) were transferred onto a glass-slide and kept in place by a laser-cut acrylic chamber and cover slip. The same procedure was performed for 5% and 10% w/v GelMA (n = 3). Deionized water was used as a blank measurement. The percentage light transmittance (%T) was measured between 400 and 800 nm, as this is considered within the visible light spectrum.

### 2.2.5 Metabolic activity measurements using PrestoBlue

To quantify the proliferation of PC12 cells over time, a PrestoBlue cell viability assay was used (n = 3). PrestoBlue (ThermoFisher, MA, USA) was performed according to manufacturer's instructions. PrestoBlue uses a resazurin-based agent that can permeate the cell membrane. The metabolic activity of cells result in the resazurin being reduced to resorufin, changing the colour of the solution and this can subsequently be detected using a spectrophotometer. PrestoBlue samples were taken at constant time intervals at day 0, 3, 5 and 7 for printed and seeded GelMA scaffolds in culture medium conditions. To take the Prestoblue sample, the scaffolds were incubated for 1 hour in culture medium conditions supplemented with 20% v/v PrestoBlue (10x). Next, the medium was aliquoted to a 96-well plate in triplicate and fluorescence was measured at 544 nm (excitation) and 590 (emission) using a POLARstar Omega microplate reader (SciQuip Ltd, Shropshire, UK). Cell-free scaffolds were used as negative controls and all data was analysed according to manufacturer's protocol.

### 2.2.6 Live/Dead staining

For certain experiments, cell viability was assessed with Calcein-AM/propidium iodide (PI), which stain live and dead cells, respectively. Calcein-AM is a cell-permeable esterase substrate, which is hydrolyzed by esterases present inside living cells. As a result, it is converted into green fluorescence. PI is an agent which is cell-impermeable, thus cannot stain living cells. However, upon loss of membrane activity, PI binds to DNA, resulting in a red fluorescence. Calcein-AM solution (final concentration 10mM) was added to the cells and incubated at standard cell culture conditions for 10 minutes. Afterwards, PI was added (final concentration 1 μg/ml) and incubated for 5 minutes. Cell viability was assessed at fixed time intervals over the course of the experiments (n = 3 for every timepoint and experimental condition).
To determine cell viability, the number of living and dead cells were counted using ImageJ software. In short, all images were converted to 8-bit. Next, the Find Maxima function was used to count the number of dead or live cells using Point Selection and an acceptable Noise Tolerance value was determined. The calculation for percentage live cells is as follows:

Percentage of Live cells = (Live Cells/Live Cells + Dead Cells)x100

### 2.2.7 Beta-III Tubulin staining

Scaffolds were cultured for a fixed amount of days in differentiation medium with cells, either seeded or encapsulated, and stained with Beta-III Tubulin in order to visualize the differentiation of PC12 cells. The constructs were fixed for 1 hour in 4% paraformaldehyde (Life Technologies). Subsequently, the constructs were washed three times with phosphate-buffered saline (PBS) and permeabilized with 100 ul Methanol: Acetone (50:50) on ice for 5 minutes. Afterwards, constructs were washed with PBS twice and blocked with 10% donkey serum with 0.1% w/v Tween-20 in PBS, referred to as blocking solution, for 1 hour. Next, the construct was incubated with mouse anti-Beta III Tubulin, the primary antibody, (COVANCE, New Jersey, USA) diluted 1:1000 in blocking solution at 4 °C O/N. The construct were washed with PBS twice and incubated with a secondary antibody, Alexa Fluo546 anti-mouse (INVITROGEN, California, USA) diluted 1:1000 in blocking solution at 37 °C for 1 hour. Lastly, constructs were washed with PBS three times, and during the second washing stained with DAPI (1:1000 in PBS) for 5 minutes at room temperature (RT). All microscope images were taken with the Zeiss AxioImager A1m or the Zeiss Axiovert 40 CSL (Zeiss, Oberkochen, Germany).

## 2.3 Neural Growth Factor incorporation

### 2.3.1 Microparticle fabrication for NGF release

To have a controlled release of NGF for directed differentiation of PC12 cells microparticles containing growth factor were fabricated. Polylactic Co-Glycolic acid (PLGA) was chosen as the base material, as it is a biocompatible and biodegradable co-polymer widely used for controlled release studies. To synthesize NGF-containing microparticles, a water-in-oil-in-water (w/o/w) protocol was followed, as already described in[72], with adaptations. 200 mg PLGA (75:25) was dissolved in 1 mL dichloromethane (DCM). The first emulsion was created by adding 50 ul of DI $H_2O$ with varying concentrations of NGF (1 ug, 5 ug and 40 ug) into the DCM and emulsifying it for 1 minute. This water-in-oil emulsion was subsequently poured into 2 mL of 1% Poly Vinyl Acetate (PVA) and emulsified again for 1 minute. The water-in-oil-in-water emulsion was then poured into 100 mL 1% PVA and after 1 minute of mixing using a magnetic stirrer 100 mL 2% isopropanol was added. After allowing for solidification of the microparticles and solvent evaporation the microparticles were washed with DI water thrice and freeze-dried until further use.

### 2.3.2 NGF concentration measurements

To measure unknown concentrations of rat Nerve Growth Factor (NGF) a sandwich ELISA (R&D Systems, Minnesota, US) was used according to manufacturer's protocol (n = 3). In short, samples containing NGF were incubated in PBS at 37 °C and aliquots were taken and replaced with fresh PBS at regular time intervals for the duration of 8 days. A 96-well plate was coated with Capture Antibody and incubated overnight at room temperature. Next, the wells were rinsed with Wash Buffer three times, and blocked with Reagent Diluent for a minimum of 1 hour. After another washing step the obtained samples and standard concentrations were added and incubated for 2 hours at RT. The washing step was repeated after which a detection antibody was added and incubated for 2 hours before performing another round of washing steps. Lastly, Streptavidin-HRP was added to each well, rinsed out with another washing cycle, and substrate solution was added to each well for 20 minutes before the addition of Stop solution. The wells were immediately analysed using a POLARstar Omega microplate reader (SciQuip Ltd, Shropshire, UK) set to determine the optical density at 540 nm and 570 nm. A standard curve was produced according to manufacturer's instructions, and the concentration of unknown samples was measured using this.

### 2.3.3 Microparticle characterization

To establish correct encapsulation of growth factors with the previously described microparticle fabrication method FITC-labelled BSA was used as a tracking dye. The fluorescence in the microparticles was checked with the Zeiss AxioImager A1m or the Zeiss Axiovert 40 CSL.
To establish microparticle size distribution microparticles are imaged after fabrication in 5ul DI Water on a glass coverslip. Different brightfield images were taken of the microparticles with a Zeiss Axiovert 40 CFC Microscope (Carl Zeiss, Jena, Germany). The images were analysed using NIH ImageJ Software. In brief, the original image is converted to a binarized image, after which the particles are counted and evaluated based on pixel scaling (suppl. Fig. 3). A minimum of 500 particles were evaluated to generate a reliable distribution of the average size of the microparticles.

### 2.3.4 SEM imaging

To investigate the microstructure of electrocompacted collagen structures with and without microparticles low vacuum SEM imaging was used (GATAN MonoCL4 system, California, US). Electrompacted collagen sheets were prepared as described in 2.1 and 2.2. To prepare the samples for SEM imaging a dehydration series was performed (10 mins DI H2O, 10 mins 50% ethanol, 10 mins 75%, 10 mins 90%, 10 mins 100%, 30 mins HHDS). Afterwards, the samples (n = 2) were coated with gold to to enable them to be used for SEM imaging.

### 2.3.5 *In vitro* cell study with microparticles

To assess the effect of NGF-loaded microparticles on cell differentiation PC12 cells were plated out with different culture conditions. The cells used for *in vitro* differentiation with NGF-loaded microparticles were kept in culture under standard conditions as described in 2.6 until start of the experiment. PC12 cells were plated out in 12-well plates at a density of 2 x $10^4$ cells/$cm^2$. At fixed time intervals bright field images were taken to check for differentiated cells. For the microparticle experimental groups, the microparticles were weighed and placed inside an Eppendorf tube with DMEM (+1% Penicillin/Streptomycin, + 1% Horse Serum) (n = 3). Every other day the DMEM was removed and placed inside the 12-well plate, and fresh medium was placed inside the Eppendorf tube. This method was chosen as putting the microparticles directly into the medium inside the well plates would have increased the aspiration of the microparticles present while changing medium.

## 2.4 Interfacing

To create a complete innervated model of the cornea ECC and GelMA were interfaced. ECC was prepared as described in 2.1.1 and GelMA was printed as described in 2.2.3, however for direct interfacing GelMA was printed onto a steelplate within a petridish to allow for direct EC on top of the GelMA scaffold. The effect of interfacing was determined through Live/Dead stainings as described in 2.2.6.

## 2.5 Statistical analysis

All data were statistically analyzed using SPSS 13.0 (SPSS, Illinois, US) and Prism 7 (GraphPad Software, California, US). $P < 0.05$ was considered statistically significant.

# Chapter 3: Results and discussion

## 3.0 Material selection

To create an *in vitro* model for the cornea, specifically focusing on innervation, various points need to be taken into consideration. First, it is important to note that there is a disparity in the optimal biomaterial for, on the one hand, mimicking the cornea and, on the other hand, providing a platform for nerve cell growth and axonal guidance. Both biomaterials have different requirements in regards to their mechanical, chemical and biological qualities. In regards to the optimal biomaterial for use as a corneal tissue equivalent, it is of importance that it has similar mechanical properties as native cornea. Furthermore, transparency of the biomaterial used should be similar to native cornea. Lastly, another important component is stability, especially taking into consideration the fact that an *in vitro* model needs to have sustained function and that nerve cells need time for axonal outgrowth to occur. The biomaterial used as a scaffold for nerve cells needs to be optimized to support the viability of neuronal cells over time, and secondly to sustain differentiation of these cells and encourage neurite outgrowth. Thus, keeping these features in mind, and to stay in line with similar work previously done in this lab, it was decided to use electrocompaction of collagen for mimicking corneal tissue and methacrylated gelatin (GelMA) bioprinting as a scaffold for nerve cells. GelMA has been used extensively in bioprinting strategies for tissue engineering, because of its beneficial properties before, during, and after the 3D printing process.[73,74] Additionally, it has been shown to be able to support the growth of a wide variety of cell types.[75] See supplemental fig. 4 for a schematic representation.

## 3.1 Electrocompacted collagen

### 3.1.1 Macroscopic analysis of fabrication

As can be seen in Figure 5, successful electrocompaction (EC) of collagen has been achieved. The successfulness of the compaction is seen through the formation of a thin sheet-like structure on the stainless steel plate. The thickness of the formed sheet is between 400 and 800 nm, which is similar to native cornea.[1] Furthermore, through macroscopic analysis it was noted that post electrocompaction cross-linking with 1mM Riboflavin improved the mechanical strength of the collagen sheet, as it is able to hold its shape while being clamped (Fig. 5B).

The most commonly used collagen for EC is type-I collagen, although some sources used type-II as well, with the voltage and duration of current application varied (3 volts for 45 min, 6 volts for 15 min or 5 A/cm$^{-2}$ for 1 hour).[62,76,77] It may be evident that for EC to move forward as a

reliable and reproducible technique, standardization of its protocol is required. To look more into the actual changes occurring during the process of EC the current against time can be plotted (Fig. 5C). The usual curve seen when electrocompacting collagen is an initial decline in current, followed by a small rise, a steep decline and eventual levelling off.

As $I = V/R$ where I = Current, V = voltage and R = resistance, the decrease and increase in current is due to the increase and decrease of the resistance of the collagen solution, respectively. A possible theory for the increase in resistance over time could be that the tight packing of collagen molecules that occurs during EC results in a dense layer that increases the relative resistance of the whole solution. Interestingly, the current (and resistance) stay constant after approx. 150 seconds, suggesting that the electrocompaction process has been completed quicker than the duration used in previous studies.[61, 62] However, this is a limited quantifiable method, and should at most be used as a relative comparison between different EC trials. Lastly, a wide variety of factors heavily influence this process, as attested by the fact that using collagen sourced from a different animal showed unsuccessful compaction in this project (data not shown). Thus, strong consideration needs to be given to the origin of the collagen (animal/synthetic), manufacturer, and type of collagen. To investigate the electrocompacted collagen as a basis for cornea mimicking certain properties need to be defined.

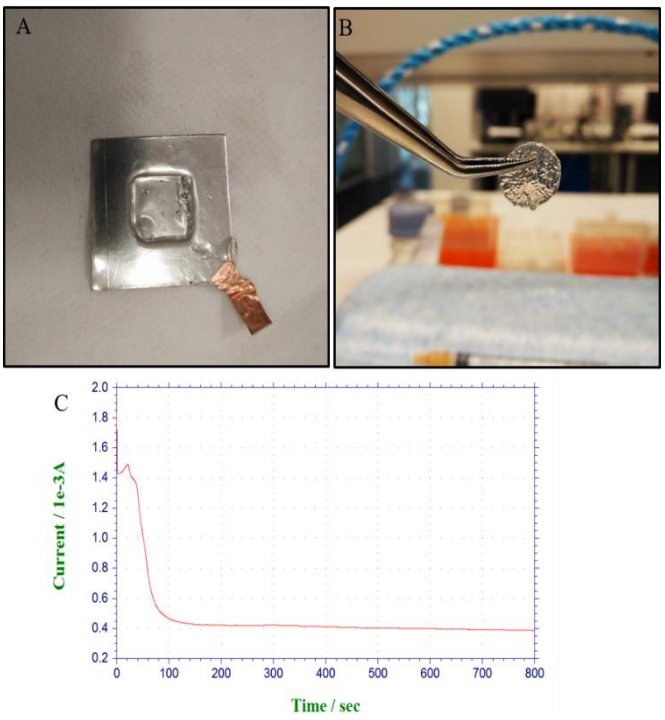


Figure 5: Electrocompaction of collagen. Pre-crosslinked electrocompacted collagen (A). After Riboflavin crosslinking (B). Representative graph of current over time for electrocompaction of collagen type I

### 3.1.2 Mechanical assessment

To examine the mechanical properties of the electrocompacted collagen post crosslinking tensile testing was performed. Figure 6A shows an example of a stress strain curve for ECC. We could not perform tensile testing on non-compacted collagen due to the softness of the material, hence the n.a. (not applicable) in the figure. The ultimate strain and ultimate stress were 19.3% and 81.5 kPa, respectively (Fig. 6C). The tensile modulus of ECC was calculated to be 0.89 MPa with a std. error of mean of 0.076 (Fig. 6B) . The Young's modulus of the ECC was 221.4 kPa with std. erorr of mean of 51.54 . In this study, tensile modulus was measured at the steepest incline, while Young's modulus was measured with the slope at the start of the curve. To note, tensile testing of conventional collagen hydrogel was not able to be performed due to inability to be clamped correctly in its wet state. However, collagen hydrogels were determined to have a tensile modulus ranging from 1 to 28 kPa according to Lopez-Garcia et al.[78] Thus, it can clearly be concluded that the process of electrocompaction drastically increased the mechanical properties of the collagen. The native human cornea has been reported to have a tensile modulus between 3-13 MPa.[79] In a different study, the Young's modulus of the human cornea was determined to be approx. 290 kPa.[80] Thus, the tensile moduli reported in this thesis converges upon the lower bound of the real tensile modulus of the native cornea, although currently still at least 3.5 fold lower, and the Young's modulus of ECC is similar to that of native cornea. All in all, this show the potential of ECC with riboflavin crosslinking as a viable option for corneal tissue engineering.

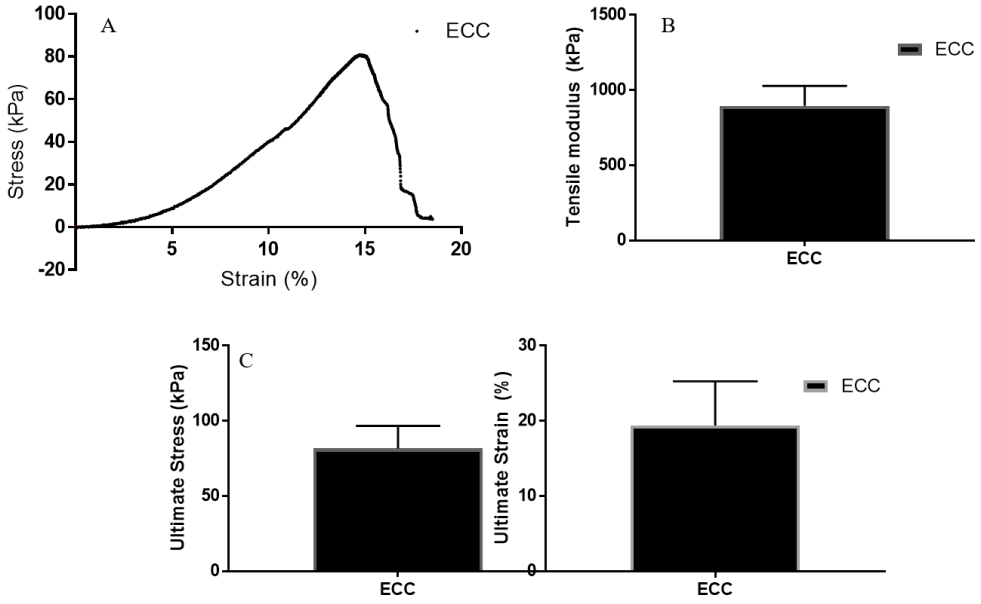


Figure 6: Mechanical assessment of riboflavin crosslinked ECC. A typical stress-strain curve displayed by tensile testing ECC (A). Tensile modulus (B). Ultimate stress and ultimate strain (C). All values are displayed in kPa and %. Error bars represent std. error of mean (SEM). (n = 3)

### 3.1.3 Transparency

To assess the transparency of the biomaterials used in this project the light transmission spectra from 400 nm to 800 nm was measured. The light transmission measurements showed that the electrocompacted collagen samples had high transparency within the visible light spectrum (Fig. 7). The values ranged from 85% at 400 nm to 92% at 800 nm. In the native cornea, transparency plays a critical role in optimal vision through light image formation. The previously mentioned values are similar to the values obtained from native cornea transparency measurements (around 80% at 380nm and more than 90% between 500 nm and 1300 nm[17]), thus showing the potential of EC collagen to mimic native cornea.[81] Comparing these results to other methods of crosslinking for ECC in literature, such as genipin and EDC-NHS, it is suggested that riboflavin crosslinking is at least as good if not superior to these other methods.[62] Furthermore, several studies using different biomaterials such as non-compacted collagen and silk films showed similar transparency.[82,83] The light transmission measurements of 5% and 10% w/v methacrylated gelatin showed very high transmittance percentages. The values ranged from 88% at 400 nm to 97% at 800 nm (Fig. 7). These results taken together show the potential of using a construct that combines both GelMA and ECC as an *in vitro* model for the cornea, while maintaining transparency throughout.

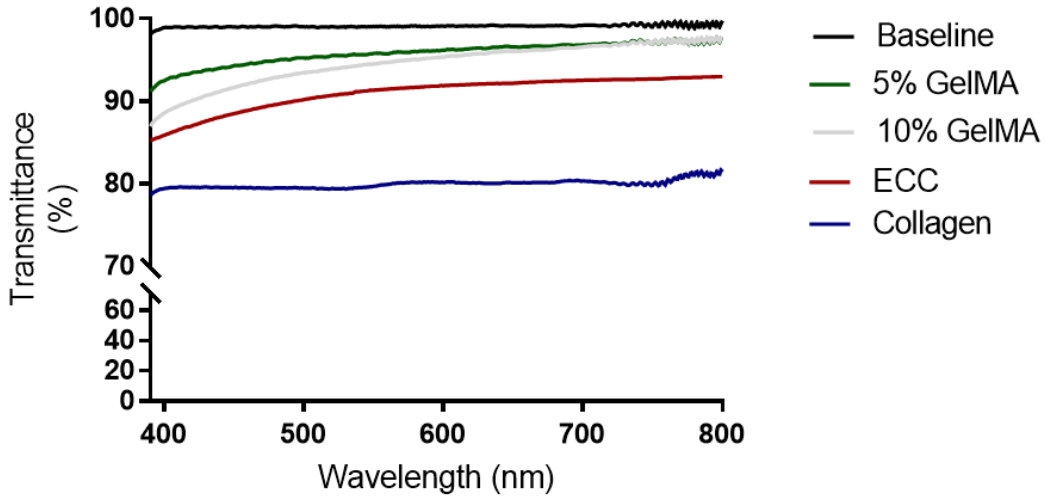


Figure 7: Representative light Transmission spectra from collagen and GelMA samples over the visible light spectrum. The light transmission spectra of the biomaterials was measured continously between 390 nm and 800 nm and compared to a baseline of DI $H_2O$. The average of n = 3 was taken for all samples. ECC = electro compacted collagen post-crosslinking, gelMA = gelatin methylacrylade

### 3.1.4 *In vitro* passive degradation assessment

Bioengineering *in vitro* models of organs present in the native human body requires certain considerations, one of these being the long-term stability of the construct. Degradation was

assessed by means of polymer dry weight after soaking in DMEM for a fixed duration of time. For this study, it was chosen to aim for a material that would be stable for at least a period of 14 days.

The collagen samples used were electrocompacted at 5 volts for 400 seconds, with post cross-linking with 1 mM riboflavin solution. Figure 8 shows the changes in dry weight of ECC taken at multiple time points. The dry weight slightly decreased from 6.05 ± 0.21 mg on day 0 to 5.85 ± 0.64 mg on day 14. The dry weight of ECC appears to have some level of inter-variability. As mentioned in 2.3, the graphical representation of the current over time shows slight differences between samples, this slight difference could result in a slight change in structure of the ECC and hence in the dry weight. Secondly, the ECC was soaked in DMEM for the duration of this experiment. The samples thus could have gained additional weight through ions present, hence the higher dry weight measurement at day 4. Kishore et al. showed that ECC was able to withstand active degradation with collagenase treatment significantly longer compared to non-compacted collagen. [62] Furthermore, post cross-linking drastically increased the stability of the collagen. All in all, these results indicate that electrocompacted collagen has sufficient stability to be used as a cornea-mimicking material in long-term *in vitro* studies.

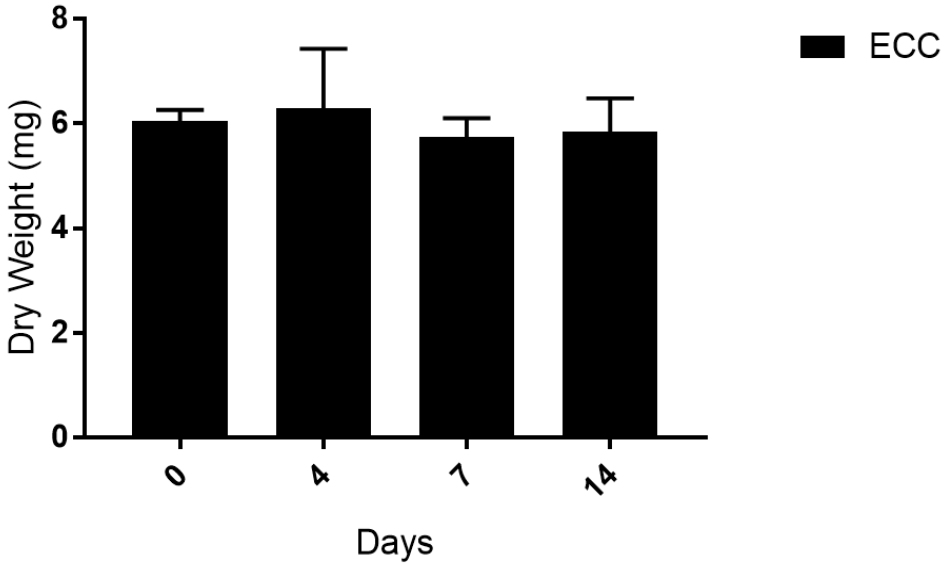


Figure 8: Passive degradation assessment of electrocompacted collagen samples by means of dry polymer weight. Data is presented in mean ± SD (n = 2).

## 3.2 Bioprinting

### 3.2.1 Pilot study – PC12 density optimalisation

To introduce neuronal innervation into the model, PC12 cells were chosen as the appropriate cell line. Historically this cell line has been used extensively in relation to neuronal models.[84,85] As a proof of concept, we showed successful differentiation of PC12 cells on plastic culture plate substrate. PC12 cells started to show neurite outgrowth from day 1 onwards, and in subsequent days neurite outgrowth increased in length and abundance (Fig. 9). The microscopic analysis showed that a non-confluent cell seeding density allowed for neurite outgrowth, while the difference between 2000 cells/cm$^2$ and 4000 cells/cm$^2$ was minimal. Furthermore, it can be seen that PC12 cells exhibit the tendency to aggregate and cluster together. This cell behavior could influence the outgrowth of neurites, due to cells 'blocking' each other from growing neurites. The lower seeding density preference has been taken into account in all subsequent experiments.

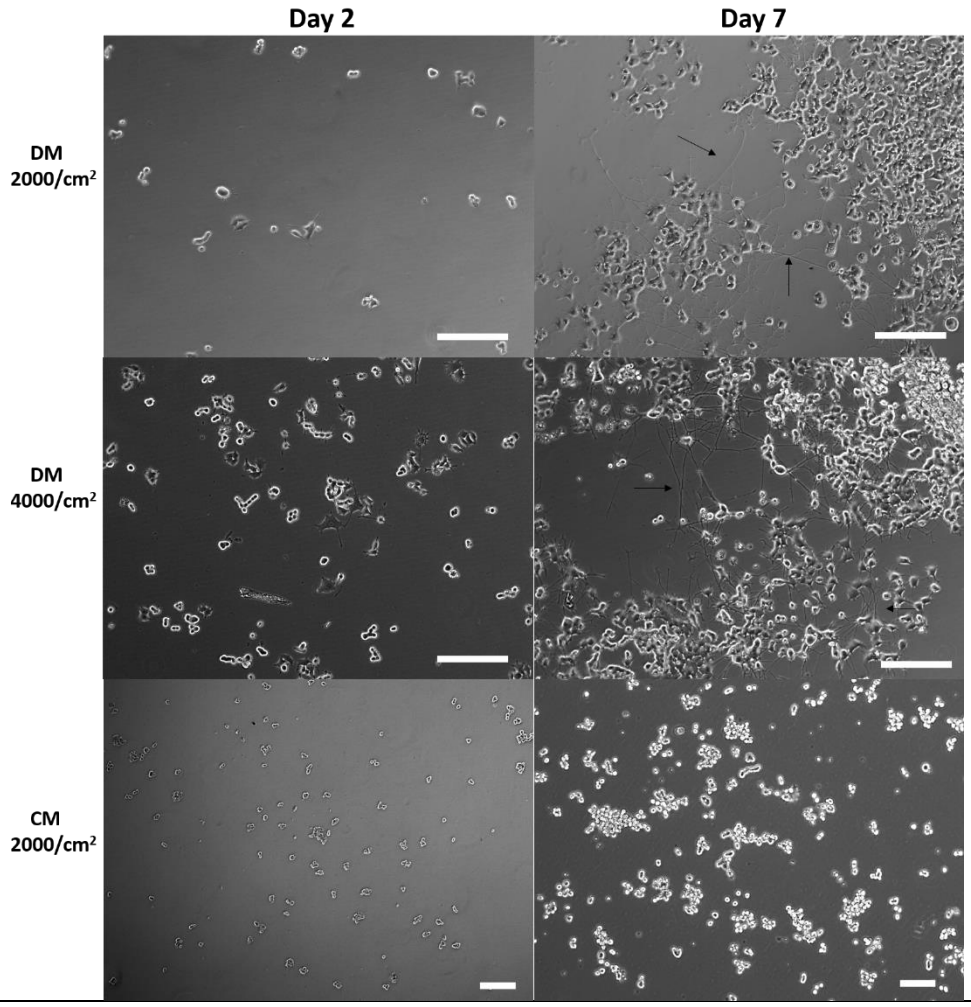


Figure 9: Optimizing differentiation density of PC12 cells on plastic culture substrate. Arrows indicate extensive neurite outgrowth in the differentiation conditions. Scale bar = 200 um. DM = Differentiation medium, CM = Culture medium

### 3.2.2 Optimalisation bioprinting parameters

Preliminary printing was performed to find the optimal printing parameters for high fidelity prints. Due to the extensive characterization of GelMA in regards to its rheological properties in literature it was chosen to not include a confirmation of these studies (i.e. rheological evaluation of 10% w/v GelMA) in this thesis.[86,87] Furthermore, optimalisation of the printing parameters was relatively straightforward, thus no rheological trouble shooting with printing was needed. Suppl. Fig. 5 shows the microscopic pictures representing different printing parameters. The bioprinter was programmed to print the construct directly into a petri dish. After optimizing steps the final parameters for printing of 10% w/v GelMA (0.06% LAP) were: 6 mm/s printing speed, 23 °C cartridge temperature and 2.5 bar pressure for extruding. Additionally, the stage was cooled to 10 °C to aid GelMA in retaining its shape post printing. Finally, the prints were crosslinked for 60 seconds with 365 nm UV-light. As is expected, slower speed of printing as well as higher pressure increased the strut diameter. Furthermore, increasing the temperature of printing led to GelMA being extruded in a more liquid form, resulting in a decrease of printing fidelity.

### 3.2.3 Microscopic and Live/dead analysis of 3D printed GelMA

Microscopic pictures of day 1 after printing show cells present in printed and seeded constructs (Fig. 10). Notably, the PC12 cells still exhibit the tendency to aggregate, and are not uniformly distributed through the scaffold. The presence of live cells inside the printed structures were confirmed by a live/dead assay 1 day after printing (Fig. 11). Cell viability 1 day post printing was 29.9%, which was later optimized in 3.4.2. The relative amount of live cells decreased compared to cell counts taken post-harvesting from the culture flasks before encapsulation and printing occurred (as confirmed by trypan blue). Generally, it is known that cell viability is decreased during the printing process.[88] The slightly harsh conditions that the cells undergo before, during and after the printing procedure can result in cell death. For example, cross-linking with UV-light post printing is required in the use of GelMA as a method of stabilizing the printed structure. However, this can have detrimental effects on cell viability. Overall, the aim of this experiment was to confirm alive cells to be present, and although viability should be optimized in the future, live cells have been confirmed to be present within the scaffolds.

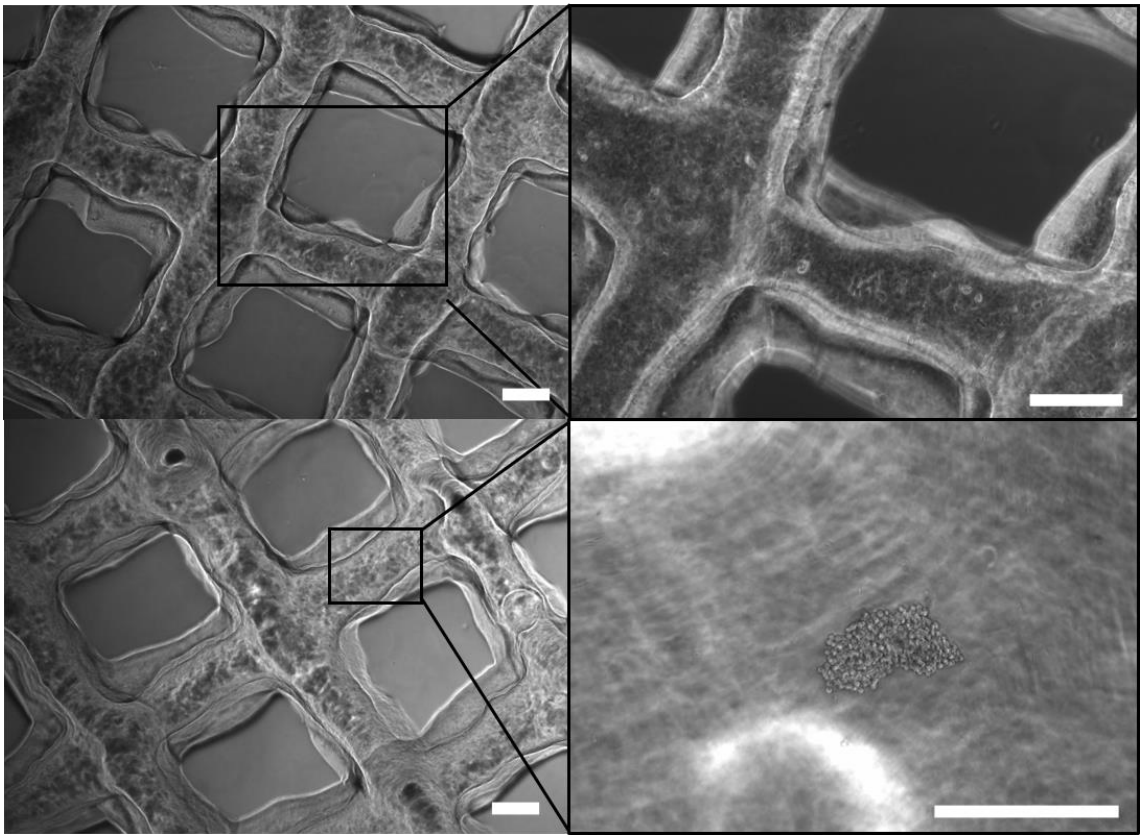

Figure 10: Microscopic analysis of printed and seeded 10% w/v GelMA scaffolds 1 day post printing. Printed scaffold (top)). Seeded scaffold (bottom). scale bars = 200 um

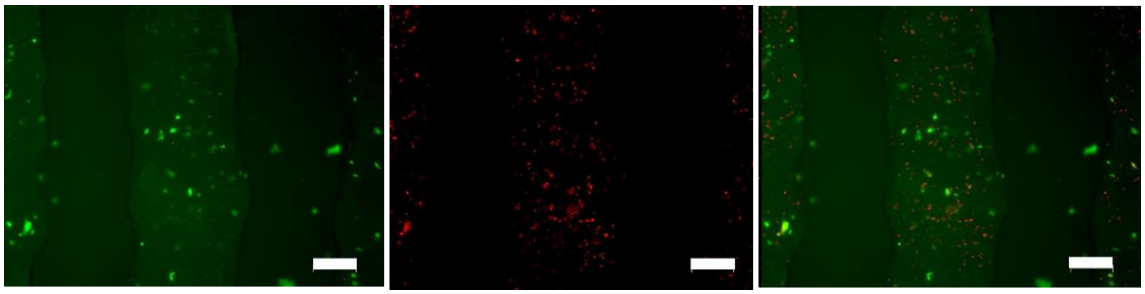

Figure 11: Live/dead staining of PC12 cells bioprinted within 10% w/v GelMA 1 day post printing. Live (left), dead (middle), and merged (right). Calcein AM/PI was used to stain the live (green) and dead (red) cells, respectively. Scale bar = 200 um

### 3.2.4 Metabolic activity of PC12 cells

The metabolic activity of the PC12 cells both in seeded and printed constructs was also assessed. PrestoBlue samples were taken over a period of 7 days, every other day. Data is represented in absorbance measured, which relates directly to metabolic activity. Figure 12 shows a very slight decrease in relative metabolic activity of 11.7% from day 1 to day 7. PrestoBlue assays show solely the total metabolic activity of the cells, which is a mixture of cell proliferation, cell size, metabolic rate and cell survival. Thus, it is hard to draw definitive conclusions on the results. It could be that the cells present at the start were stagnant in regards to proliferation, possibly due to being encapsulated resulting in a relatively stiff 3D environment. This hypothesis holds some weight considering the preference of neuronal cells for a soft environment.[89] On the other hand, it could be that the rate of cell proliferation and cell death are similar, resulting in a similar metabolic activity over time. In either case, the presence of living cells was confirmed in the printed scaffolds for the whole duration of the experiment.

The seeded scaffolds showed a surprising significant decrease of metabolic activity within 7 days, with a 65.8% reduction in metabolic activity compared to day 1 ($p<0.05$). PC12 cells adhere lightly to uncoated substrates, including plastic culture flasks, as demonstrated by the lack of trypsin needed for passaging of these cells. Thus, constant medium changing could have dislodged cells partly from the scaffold, and as a result lowered the overall metabolic activity. This could be confirmed in future studies by measuring the metabolic activity of the surrounding medium to account for dislodged cells. To note, the cluster formation present with PC12 cells could influence nutrient diffusion to cells located in the center of the cluster, thus decreasing overall metabolic activity.

In future studies, it could be interesting to look at different w/v concentrations of GelMA and the effect of the softer environment on the encapsulated cells. To note, lower concentrations of solely GelMA are often incompatible with extrusion-based printing methods due to insufficient shape retention.[90] Thus, these studies should preferably be performed with molded scaffolds, rather than printed, and therefore will not be able to be directly compared to the previous data. Together, these data resulted in advancing the project with PC12 cell printed scaffolds as these showed a sustained metabolic activity of the cells. Additionally, encapsulation of cells inside the scaffold mimics native corneal tissue more closely, as the cell bodies providing the free nerve endings in the native corneal tissue are situated independently of the cornea, where only

the neurites are protruding into the cornea.[91]

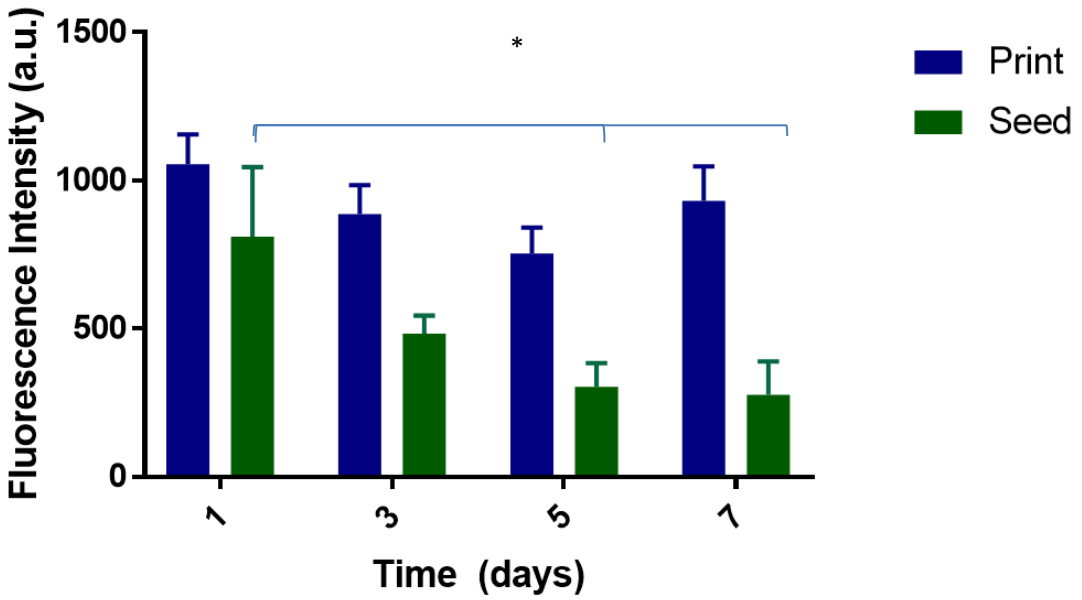


Figure 12: The effect of printing and seeding PC12 cells on their metabolic activity for the duration of 7 days measured via PrestoBlue. (n = 3) * = P<0.05

### 3.2.5 Differentiation capacity bioprinted PC12 cells

To assess the differentiation capacity of bioprinted PC12 cells within 10% w/v GelMA scaffolds cells were stained with Beta-III Tubulin, which is specifically localized in neurons. The cells were kept in differentiation medium for 12 days before staining, refreshing the medium every other day. As can be seen in Figure 13, PC12 cells were able to have some level of neurite outgrowth. It can be seen that outgrowth of neurites is relatively limited compared to the multi-directional outgrowth as seen on 2D plastic substrates (see 3.8.1). In 2D, the neurites are able to freely spread outwards (not inhibited by a surrounding hydrogel). However, this is not representative of the native 3D environment. The relatively dense 3D network of GelMA can hinder new neurite outgrowth from occurring.

Interestingly, the neurites seemed to be topographically guided to extend along the printed struts. However, for the incorporation of bioprinted neuronal cells into a *in vitro* model of the cornea it is required to have guidance cues towards the ECC. Although the topographical cues from the printed scaffold allow for a semi x/y-directional guidance of neurite outgrowth, to sustain z-directional outgrowth a different technique is required. Recently, it has been shown that a NGF concentration gradient can guide neurite outgrowth in PC12 cells within a p(HEMA) hydrogel.[92] Thus, a method for sustained release of NGF from the electrocompacted collagen was investigated for the progress of this research project.

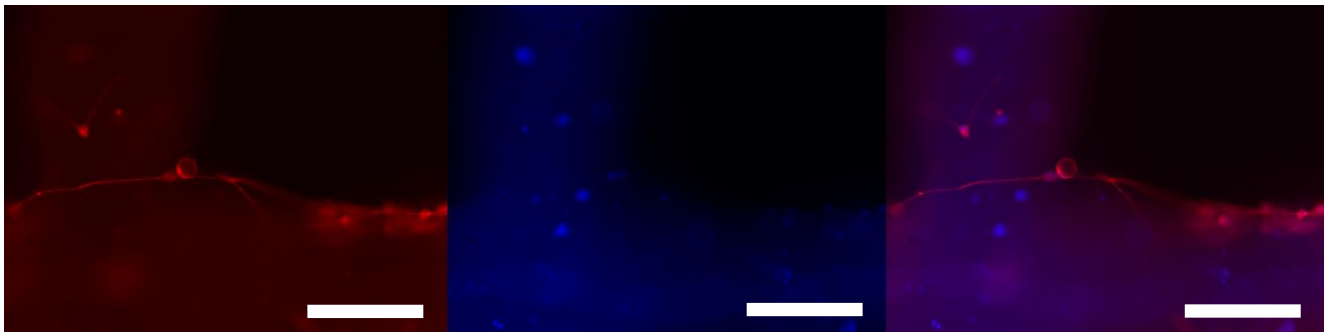

Figure 13: Beta-III tubulin staining of PC12 cells printed within 10% w/v GelMA after 12 days. Neurite outgrowth can be seen going along the printed scaffold. Beta-III Tubulin is displayed in red and DAPI staining is displayed in blue. Scale bars = 200 um

## 3.3 Microparticle fabrication

### 3.3.1 Microparticle characterization

To produce a directionally guided neurite outgrowth model, microparticles were used to provide for a sustained release of neural growth factor (NGF). The chosen material for these microparticles was Poly-Lactic Co-glycolic Acid (PLGA), a widely used co-polymer that is biodegradable and biocompatible.[93] To fabricate microparticles loaded with NGF a Water-in-oil-in-water (w/o/w) emulsion protocol was followed, adapted to the available lab equipment. As a proof-of-concept, microparticles loaded with FITC-BSA, a fluorescent protein, were fabricated using different experimental conditions. This technique resulted in spherical microparticles with FITC-BSA loaded inside, as confirmed by fluorescent microscopy (Fig. 14). The fluorescence is limited to the volume inside the microparticles, thus showing successful encapsulation.

Furthermore, we investigated the effect of PVA concentration and/or PLGA concentration on the characteristics of the microparticles, focusing on the size of the particles. Histograms of the size distributions for the different conditions can be found in Figure 15. The smallest average microparticles size was 20.10 um , using a concentration of 20% PLGA and 1% PVA (Table 1). Decreasing the PVA concentration, and/or decreasing/increasing the PLGA concentration led to microparticles with a larger size or larger standard error. Additionally, an increased precipitation was found when increasing the PLGA concentration to 25%. Therefore, for future use it was chosen to continue using the 20% PLGA 1% PVA microparticles.

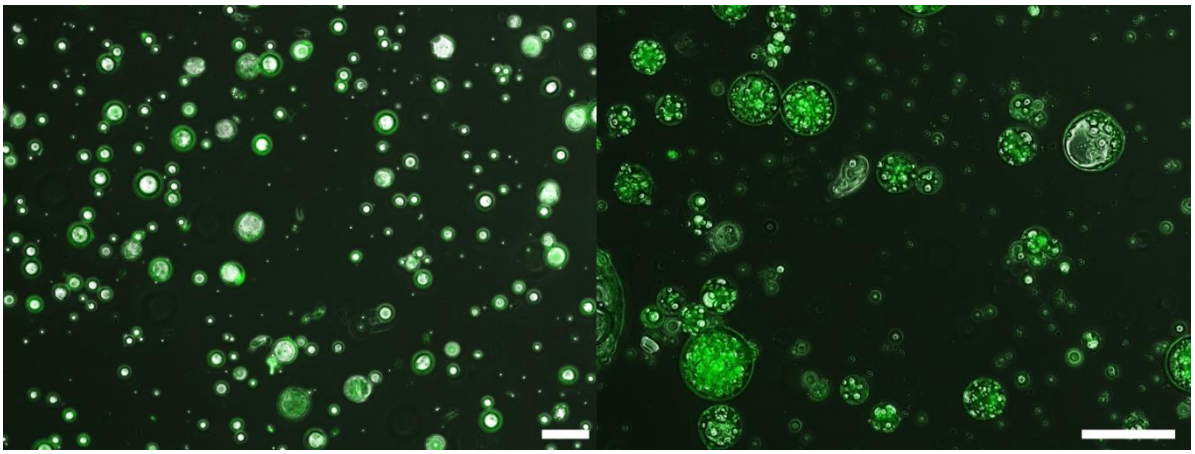

Figure 14: Representative fluorescent microscopy pictures of w/o/w PLGA microparticles in aqueous solution at low (left) and high (right) magnification showing the spherical morphology and successful encapsulation of FITC-BSA within the microparticles. Scale bars = 200 um

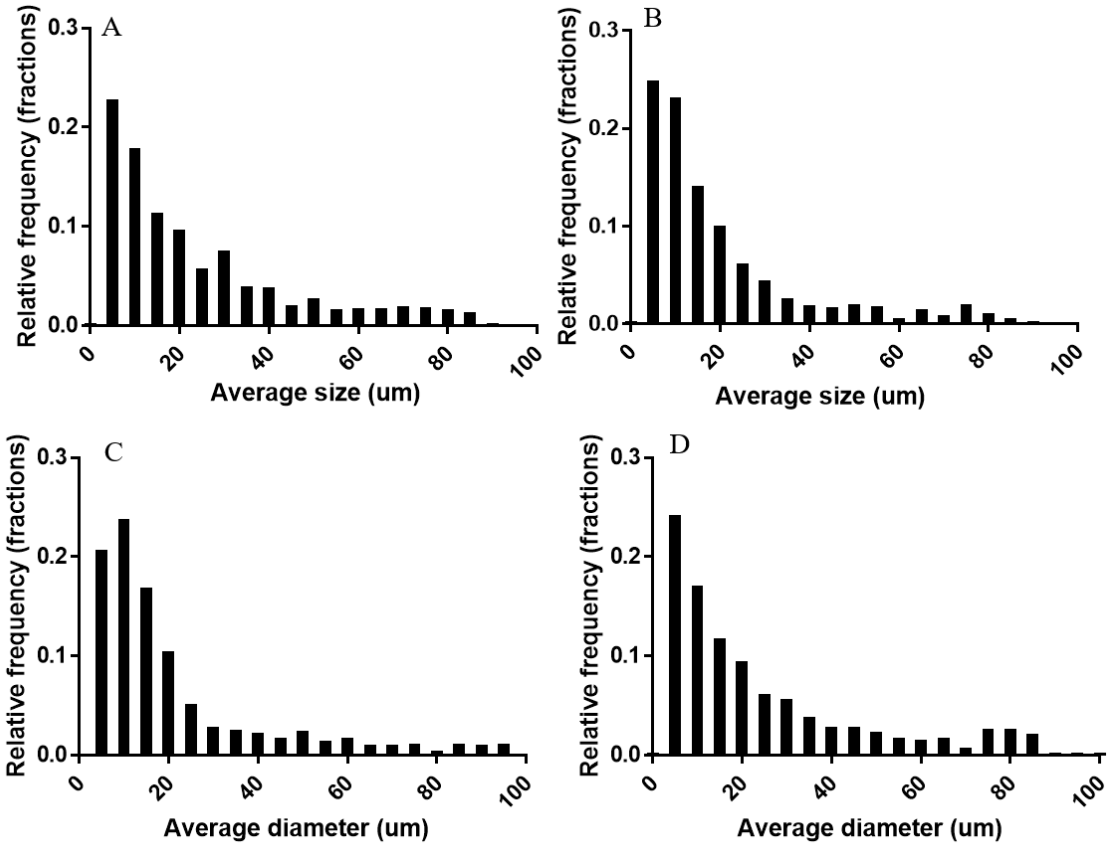


Figure 15: Size distribution by fraction of growth factor loaded PLGA microparticles sized using ImageJ software. 0.5% PVA, 10% PLGA (A). 1% PVA, 20% PLGA (B). 0.5% PVA, 20% PLGA (C). 1% PVA, 25% PLGA (D).

Table 1: Average sizes of the microparticles produced with different concentrations of PVA and PLGA. All values are represented as mean with std. error of mean

| Microparticle fabrication method | 0.5% PVA 10% PLGA | 0.5% PVA 20% PLGA | 1% PVA 20% PLGA | 1% PVA 25% PLGA |
|---|---|---|---|---|
| Mean size (um) | 23.96 ± 0.59 | 22.21 ± 0.84 | 20.10 ± 0.60 | 24.47 ± 0.97 |

### 3.3.2 Release studies of NGF microparticles

To assess the growth factor release profile of the optimal particle formulation, an *in vitro* release study was performed in PBS at 37 °C using ELISA (fig. 16). For each group, 5 mg of NGF-loaded microparticles (NGF:MP) was used to measure the amount of NGF released for 8 days. Two different loading concentrations were measured: 5 ug and 1 ug loading (per 200 mg PLGA). During the first 6 hours a fast release can be seen, with 16.80% and 22.56% of the total NGF released in the 5 ug and 1 ug loaded groups, respectively. After 24 hours the relative NGF released was 31.8% for 5 ug loading and 54.1% for 1 ug loading. This spiked release leveled off over the course of 24 hours after which a steady state release was observed for the remainder. The total amount of NGF released after 8 days was 1.8 ng for 5 ug loading and 0.74 ng for the 1 ug loading group. The initial high burst release of NGF can be explained by the growth facgtor not being completely encapsulated within the microparticles, but rather being located near/ bound to the surface of the microparticles. Important to note, the encapsulation efficiency reached with these experiments is rather low, 5.6% and 1.97% for 1 ug and 5 ug loading, respectively. Previous work in the institute proved troublesome to encapsulate NGF and maintain bioactivity. For future studies, it would be important to optimize the encapsulation efficiency of the microparticles. To summarize, encapsulation of NGF within PLGA microparticles has been proven, and sustained release has been confirmed.

### 3.3.3 *Ìn vitro* cell assay NGF microparticles

To investigate the bioactivity of the NGF:MP, it is necessary to prove their capability to differentiate neuronal PC12 cells *in vitro*. To this extent, aliquots of high-glucose DMEM (+1% P/S, +1% HS) with NGF eluted by 15 mg of 1 ug loaded MPs and 15 mg of 5 ug loaded MPs were added to PC12 cells every other day. As a negative control empty microparticles were used together with DMEM (+1% P/S, +1% HS). As expected, PC12 cells cultured in differentiation medium showed long protruding neurites on day 9. Furthermore, the change of morphology from rounded cells towards a more neuronal lineage is clearly visible at day 5, as well as some initial small neurite outgrowth. 5 ug NGF:MP showed signs of differentiation after 9 days in

culture, with some small neurite outgrowth and a change of morphology in a vast number of cells (see black arrows). 1 ug NGF:MP showed very little signs of differentiation, with rare occurrences of morphological changes, even after 9 days. The NGF released from the MPs show sufficient bioactivity for changing the morphology of PC12 cells towards a more differentiated lineage. Nevertheless, it is not to an extent that is seen in the positive control. As the end goal is to use the microparticles in an innervated model wherein neurite outgrowth has to be directed, the current capacity of differentiation was deemed insufficient. To reach an appropriate amount of NGF release, future investigations used an increased loading concentration (40 ug loading per 200 mg PLGA).

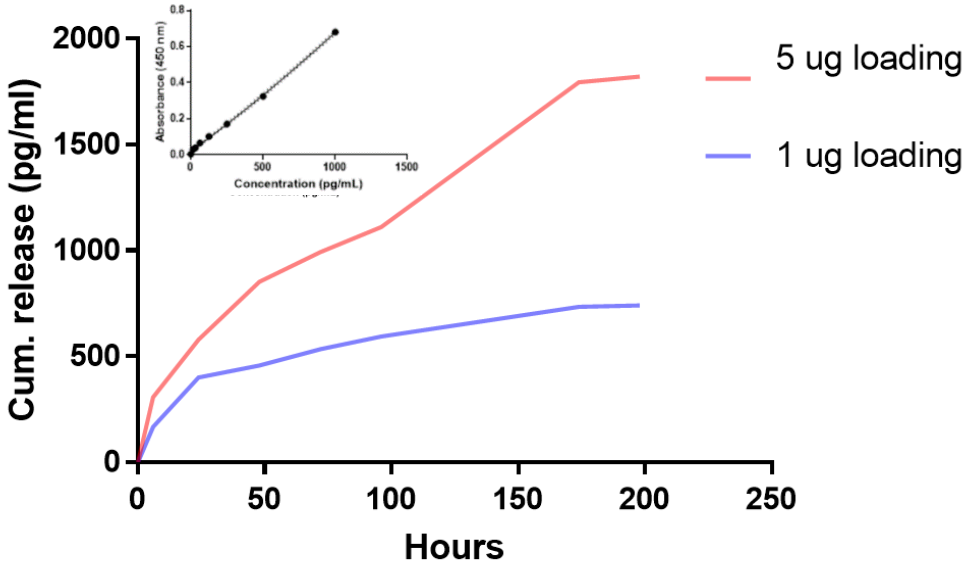


Figure 16: Release curve showing the absolute cumulative release of neural growth factor from the 0.5% PVA 20% PLGA microparticles over a period of 8 days. Growth factor release was quantified using ELISA through generating a standard curve (top left) and fitting the unknown data points after subtracting background absorbance. All measurements were taken in triplicate.

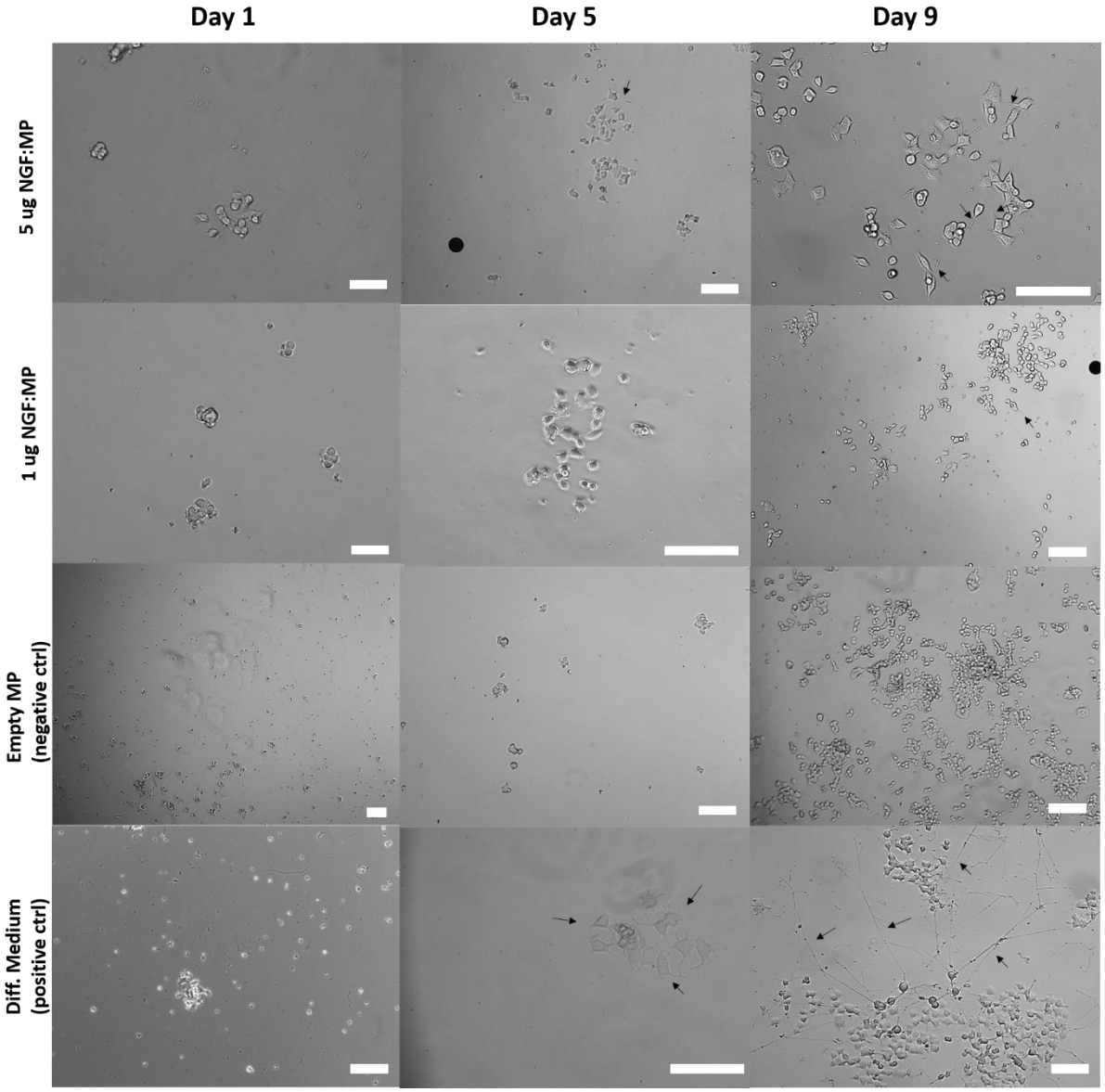


Figure 17: Optical microscopic pictures displayed the behavior of the PC12 cells after culturing with or without NGF:MPs and empty control microparticles for the duration of 9 days. Black arrows indicate morphological changes and neurite outgrowth. Black dots are microparticles present in the medium. The positive control shows clear neurite outgrowth from the PC12 cells, with increasing length from day 5 to day 9. The negative control shows no neurite outgrowth at all after 9 days, consistent with conventional morphological presence of PC12 cells not stimulated by NGF. Microparticles loaded with 5 ug (5 ug NGF:MP) can induce neurite outgrowth after 9 days, but not to the same extent as differentiation medium. Microparticles loaded with 1 ug (1ug NGF:MP) induce very scarce neurite outgrowth from PC12 cells. Scale bars = 200 um

### 3.3.5 Incorporation of microparticles into ECC

After establishing the ability of the MPs to sustain the release of NGF, efforts were undertaken to incorporate them into the electrocompacted collagen (ECC). This would allow the NGF to be released in a sustained manner from the cornea-mimicking structure (ie. the ECC), ultimately guiding the neurite outgrowth towards this structure. Firstly, the ratio of microparticles:collagen was investigated. A balance has to be found between large amounts of microparticles being incorporated for maximum release of growth factors, while maintaining the beneficial mechanical properties of the electrocompacted collagen layer. Three different concentrations of microparticles/mL of collagen were investigated: 2 mg/mL, 5 mg/mL, and 10 mg/mL. Macroscopic analysis indicated that 2 mg/mL and 5 mg/mL did not affect the strength of the electrocompacted collagen sheet compared to the negative control while 10 mg/mL seemed to affect the formation of a dense sheet of collagen. Scanning Electron Microscopy (SEM) was used to further examine the structural changes that occurred during EC. Fig. 18A shows ECC without incorporation of MPs, the aligned collagen fibril structure characteristic for ECC can be seen by the parallel grooves present. The MPs seem to disrupt the alignment of the collagen fibers, particularly in higher concentrations. Fig. 18E shows a high magnification image of the disruption of the smooth surface of the ECC due to microparticle incorporation. These results show the potential of providing a sustained release of NGF through incorporation of MPs inside ECC (NGF:MP:ECC).

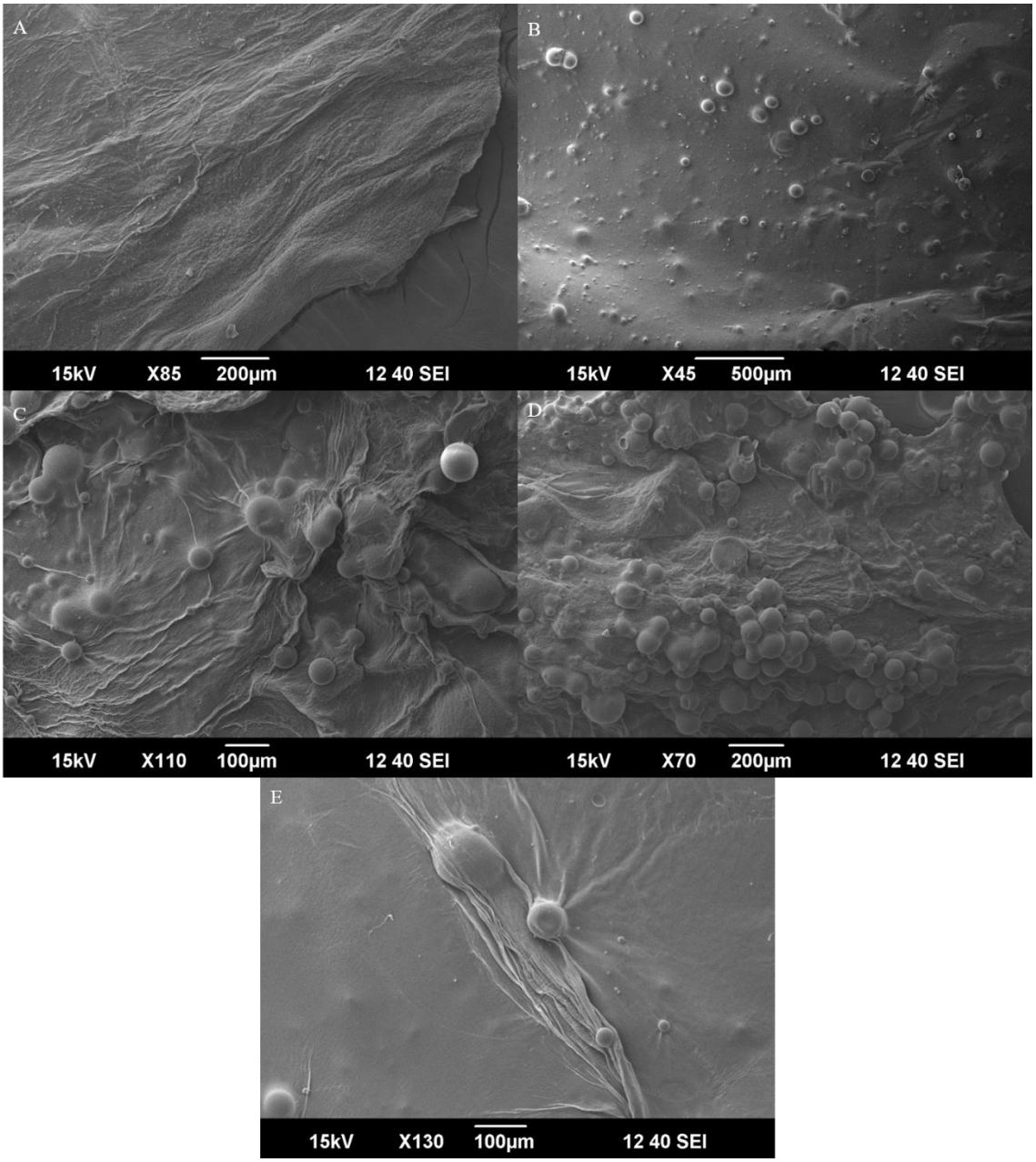


Figure 18: Representative scanning electron microscopy (SEM) images of electrocompacted collagen without microparticles (A), with 5 mg/mL microparticles (B) and 10 mg/mL microparticles (C, D). (E) shows the disruption of ECC due to microparticle incorporation. Scale bars as indicated.

## 3.4 Innervated model

### 3.4.1 Interfacing EC and GelMA

To combine both techniques and biomaterials into one single construct multiple avenues of interfacing have been explored. Logically, there are three different options to explore:
(i) Electrocompaction of collagen into a pre-existing 3D printed GelMA scaffold.
(ii) 3D print a scaffold into pre-electrocompacted collagen.
(iii) Fabricate both constructs separately.

For the first option, one of the integration approaches that can be taken is printing the GelMA scaffold onto the stainless steel plate, after which the EC chamber can be built around the scaffold and subsequently the collagen solution can be loaded into and compacted directly on top of the GelMA (Suppl. Fig. 6). Preliminary testing using a strong and rigid polycaprolactone (PCL) scaffold, showed potential. The porosity and height of the scaffold was important for the quality of electrocompaction. Due to this, it was chosen to print 3 layers of GelMA (160 um/layer) with 1.5 mm spacing between strands. A Live/Dead staining was performed to assess the effect of electrocompaction on cell viability. To identify whether cell death occurs due to application of an electrical current or the protocol in general (i.e. printing onto a stainless steel plate and lack of nutrients), another experimental group was added with the same procedure except for the application of an electrical current. Figure 19 shows the live/dead staining for the various experimental groups. Cells located on the inside of the scaffold did not survive the process of electrocompaction, as displayed by 7.8% cell viability (Fig. 19A). However, cells encapsulated in the outside of the scaffold seemed to have a higher chance of survival, with a cell viability of 62.45% (fig. 19B). The procedure without electrical current also resulted in slightly lower cell viability compared to complete control (66.1% and 74.9%, respectively). Thus, this interfacing approach does not seem optimal. Furthermore, one of the advantages of printing compared to casting is to allow for relatively rapid nutrient diffusion throughout the scaffold due to macroscopic porosity. By compacting collagen into the scaffold this advantage is neutralized, as the pores are filled by the collagen solution. These results taken together show that this option is unfavorable for the aim of this project.
The second potential approach has not been explored experimentally. Firstly, the surface of ECC is not completely flat, which makes it difficult to print on. Secondly, the current protocol requires keeping the printed cells in expansion medium for 24 hours, as they are quite fragile after the printing procedure. This would not be possible with this option, as the ECC-MP will elute NGF from day 0 onwards. All taken together, this option was deemed not optimal and thus option (iii), fabricating both components separately, was currently used for the creation of the innervated model.

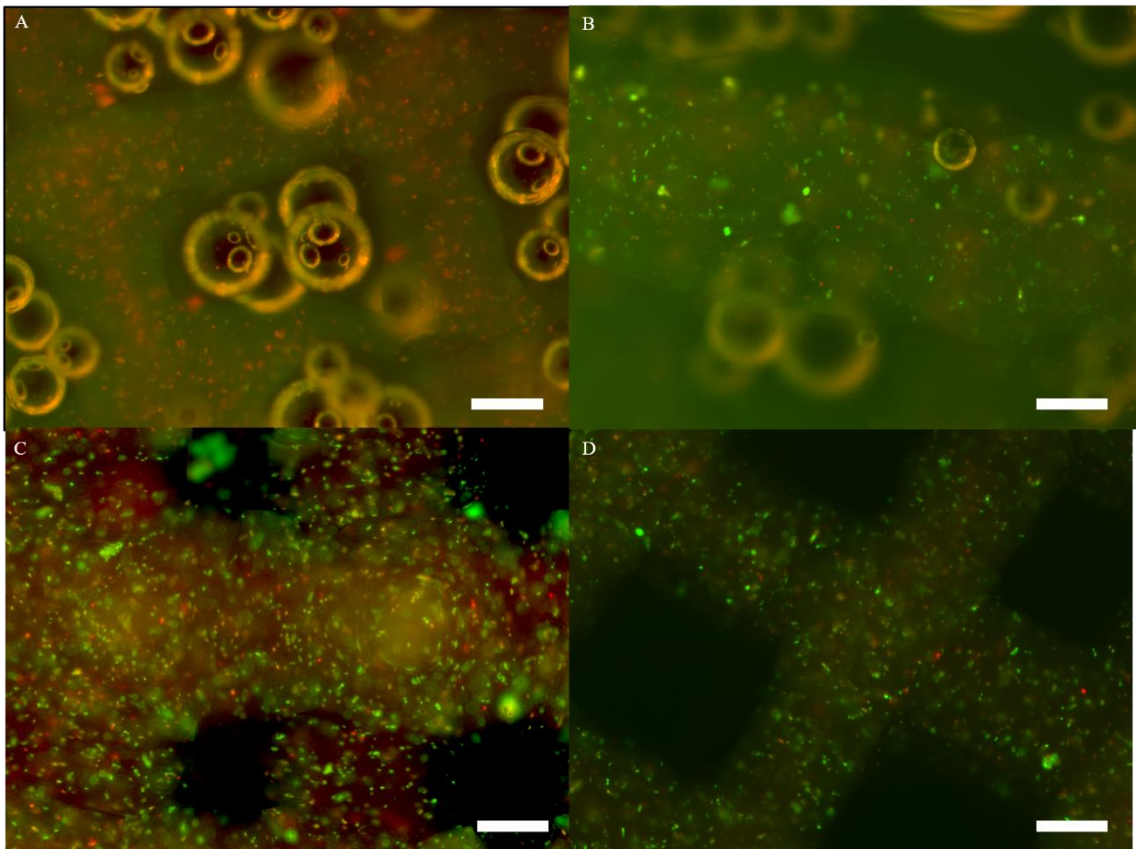


Figure 19: Live/Dead stainings of PC12 cells within 10% w/v GelMA. (A) middle of scaffold after electrocompaction of collagen. (B) Top of scaffold after electrocompaction of collagen. (C) Middle of the scaffold after undergoing the procedure without applying current. (D) control scaffold. Calcein/PI was used to stain alive (green) and dead (red) cells, respectively. Scale bars =

### 3.4.2 Neuronal guidance within interfaced innervated model

To reiterate, the innervated *in vitro* corneal model was fabricated by combining both biomaterials post-fabrication. First, to show the optimizing of the printing parameters for cell viability compared to the first print a live/dead staining was done 24 hours and 7 days after printing. As can be seen in Figure 20, 24 hours after printing cell viability was 82.4%. It should be taken into account that before printing viability was 92% as calculated by Trypan Blue. Thus, a decrease in viability of less than 10% due to printing is better compared to previously in 3.8.2.

NGF:MP:ECC did not show sufficient differentiation for encapsulated PC12 cells within a 10% w/v GelMA scaffold (Fig. 21). Thus, for the overall model currently the differentiation capacity of the PC12 cells after printing was insufficient after culturing for 7 days. The positive control (bioprinted PC12 cells with standard differentiation medium) showed some neurite outgrowth, indicating differentiation, (Fig. 21A, B). To investigate the cause of this issue, two more conditions were tested. First, a 10% w/v GelMA 3D printed scaffold seeded with PC12 cells was analysed to investigate whether the PC12 cells were able to differentiate with GelMA as a

substrate. This showed more extensive neurite outgrowth (Fig. 21 E, F). Cells can clearly be seen to sprout multiple neurites in all directions. Thus, clusters of PC12 cells are able to differentiate when seeded on top of a GelMA scaffold. Secondly, PC12 cells were seeded on NGF:MP:ECC to assess whether the NGF released from incorporated microparticles was sufficient for differentiation. The PC12 cells show extensive neurite outgrowth and differentiation (Fig. 21 G, H). This indicates that the primary cause for the lack of differentiation in the complete model is the encapsulation within a relative rigid hydrogel. In literature, differentiation of neuronal cells occurred primarily in collagen-based hydrogels.[96,97] Research within this institute initiated investigations on modified gellan gum with PC12 cells, which proved relatively unsuccessful, as gellan gum based hydrogels were not able to show extensive differentiation of PC12 cells.[98] Thus, the presence of a soft collagen hydrogel seems critical to differentiation of PC12 cells. For future investigations, a co-axial set-up could be used to fabricate constructs with an inner core of collagen, providing neuronal support, and an outer shell of GelMA, providing structural support.

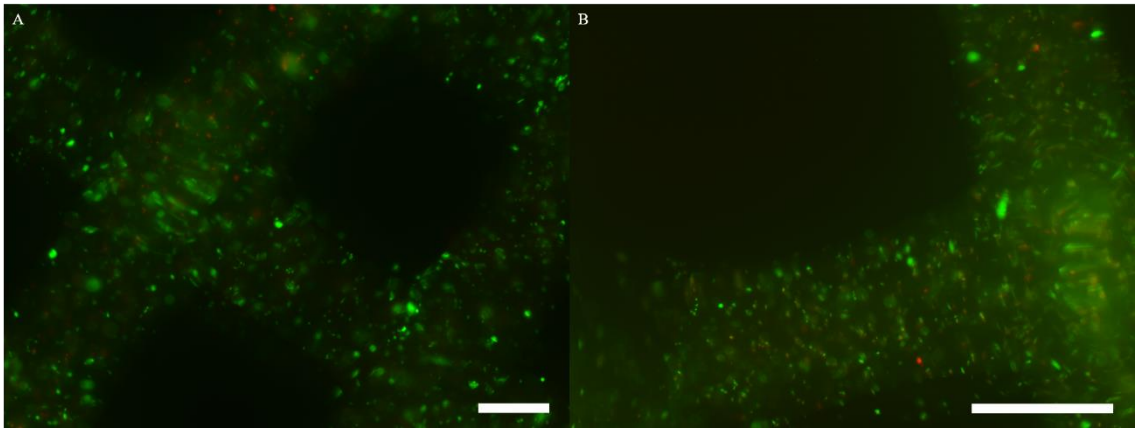


Figure 20: Live/Dead staining's of PC12 cells within 10% w/v GelMA after optimizing the effect of printing on cell viability after 1 day (left) and 7 days (right). Scale bars = 200 um

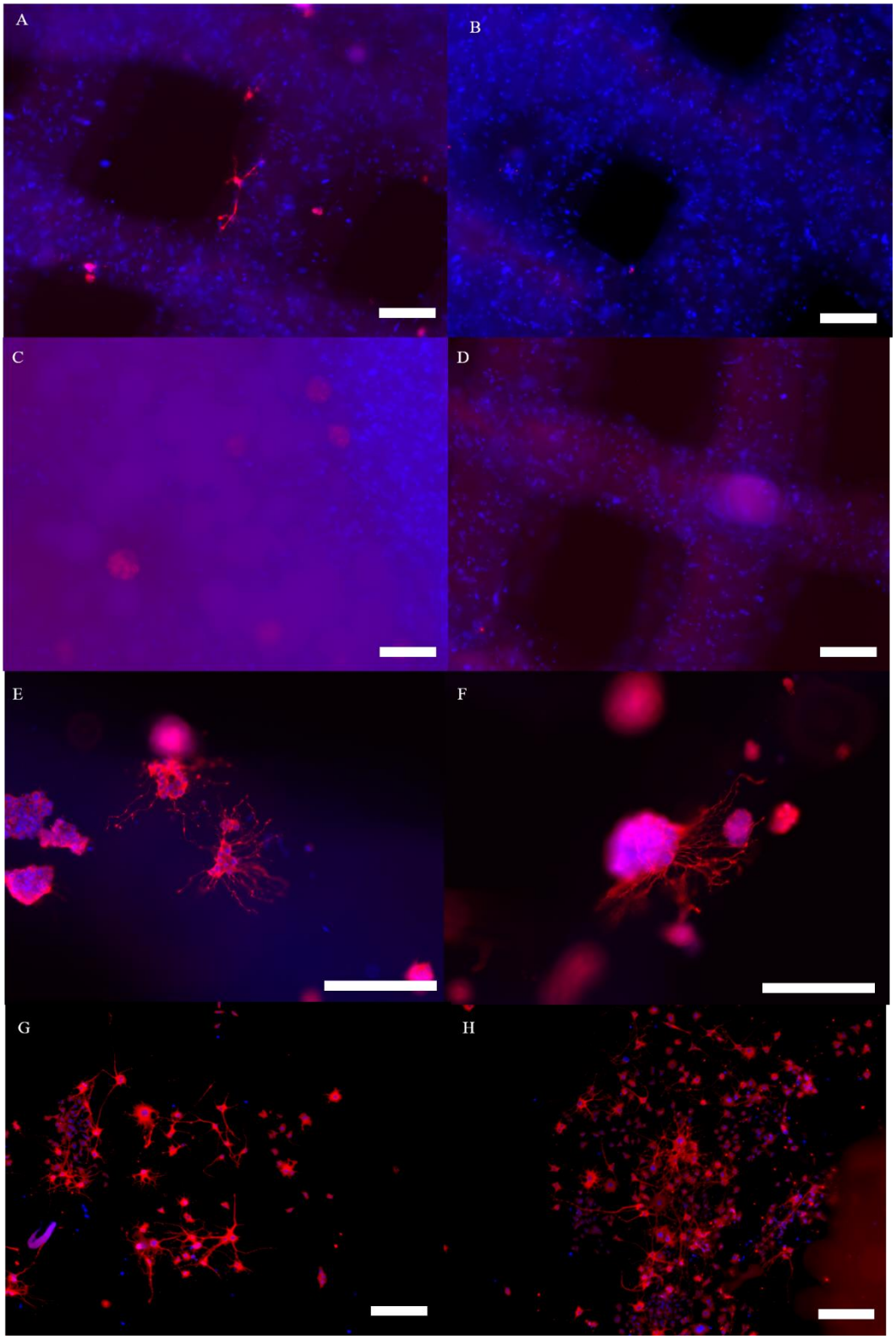


Figure 21: Beta-III tubulin staining of PC12 cells within the interfaced innervated model. Cells outgrow few neurites when NGF is dispersed within the medium (A, B). No sign of neurite outgrowth present in the interfaced innervated model of ECC:MP with 10% w/v GelMA (C, D). Neurite outgrowth can be seen extensively when seeded on top of 10% w/v GelMA (E, F), or when cultured with NGF:MP:ECC (G, H) . Beta-III Tubulin is displayed in red and DAPI staining is displayed in blue. Scale bars = 200 um

## 3.5 Conclusion and future perspectives

This project aimed to create an *in vitro* innervated model of the cornea. For this purpose, electrocompacted collagen was investigated as a basis for corneal mimicking. By examining the process of electrocompaction we showed the creation of a dense layer of collagen, with similar thickness to the cornea, and recapitulating partly the unique structure of dense, aligned collagen lamellae found in the cornea. Furthermore, the mechanical properties of ECC was significantly better than previously reported mechanical analyses for conventional collagen hydrogels ($P<0.05$), and was converging on the mechanical properties for native cornea. The high transparency of the material and the slow passive degradation *in vitro* added to the qualities of this material for use in *in vitro* cornea models.

The bioprinting of neuronal PC12 cells has been shown for the first time. Cell viability, printing parameters and seeding density were optimized to achieve adequate scaffolds for PC12 cell survival 1 day and 7 days post printing. Additionally, to create a guided innervated model, microparticles were investigated for a sustained release of NGF. Successful encapsulation of growth factor, sustained release of NGF and 2D PC12 cell response has been achieved. Next, these microparticles were incorporated into the ECC for guidance of neurite outgrowth into the cornea mimicking structure. However, although 10% w/v GelMA has been shown to sustain PC12 survival, it did not allow for sufficient cell differentiation after encapsulation. Adapting or changing this biomaterial to allow for PC12 differentiation is critical for further progression (e.g. addition of collagen through a co-axial system).

The successful differentiation of PC12 cells with NGF:MP:ECC has potential for a variety of applications outside this project. The fabrication of growth factor incorporated microparticles has been established for a wide variety of growth factors, including VEGF and BMP-2.[94,95] Combining a dense collagen sheet with growth factor releasing properties could have potential for other tissue engineering related strategies as well, whereby the relatively strong and stable collagen scaffold can provide a platform for promoting vascular or neuronal growth both *in vitro* and possibly *in vivo* due to the incorporation of a method for sustained release. To note, high concentrations of MPs could influence the strength of the ECC, and future investigations into quantifying this effect are recommended.

Possibilities for future directions and optimizing within the scope of this project have been given throughout this thesis, but looking further ahead some exciting directions could be explored. The additional of other corneal relevant cell types would add immensely to the relevance of the model as a whole. Cell types including corneal epithelial and endothelial cells could be added through seeding on the electrocompacted collagen. It has been proposed that corneal nerves directly innervate corneal cells (including keratocytes), and thus the interaction between these cell types could be critical to cell behavior. Pre-clinical applications come into scope if these cells are added successfully. Useful applications such as ocular toxicity testing,

disease modelling, and permeation studies show that the development of representative 3D *in vitro* corneal models remains a priority in the field.

# References


1. Eghrari AO, Riazuddin SA, Gottsch JD. Overview of the Cornea: Structure, Function, and Development. *Prog Mol Biol Transl Sci*. 2015;134:7-23. doi:10.1016/BS.PMBTS.2015.04.001.
2. Brandt J. Dictionary of Eye Terminology. *Ophthalmic Surgery, Lasers Imaging Retin*. 1991;22(1):60-60. doi:10.3928/1542-8877-19910101-19.
3. Gharaee H, Abrishami M, Shafiee M, Ehsaei A. White-to-white corneal diameter: normal values in healthy Iranian population obtained with the Orbscan II. *Int J Ophthalmol*. 2014;7(2):309-312. doi:10.3980/j.issn.2222-3959.2014.02.20.
4. Ruberti JW, Sinha Roy A, Roberts CJ. Corneal Biomechanics and Biomaterials. *Annu Rev Biomed Eng*. 2011;13(1):269-295. doi:10.1146/annurev-bioeng-070909-105243.
5. Michelacci YM. Collagens and proteoglycans of the corneal extracellular matrix. *Brazilian J Med Biol Res*. 2003;36(8):1037-1046. doi:10.1590/S0100-879X2003000800009.
6. Klintworth GK. The cornea--structure and macromolecules in health and disease. A review. *Am J Pathol*. December 1977:718-808. doi:10.1002/term.2621.
7. Ethier CR, Johnson M, Ruberti J. Ocular Biomechanics and Biotransport. *Annu Rev Biomed Eng*. 2004;6(1):249-273. doi:10.1146/annurev.bioeng.6.040803.140055.
8. Yanez B, Leonard BC, Raghunathan V, Abbott NL, Murphy CJ. Interfacial properties of corneal epithelial cells at different degrees of differentiation. Investigative Ophthalmology & Visual Science. 2014 Apr 30;55(13):1482-.
9. Leonard BC, Yañez-Soto B, Raghunathan VK, Abbott NL, Murphy CJ. Species variation and spatial differences in mucin expression from corneal epithelial cells. *Exp Eye Res*. 2016;152:43-48. doi:10.1016/J.EXER.2016.09.001.
10. DelMonte DW, Kim T. Anatomy and physiology of the cornea. *J Cataract Refract Surg*. 2011;37(3):588-598. doi:10.1016/J.JCRS.2010.12.037.
11. Li F, Carlsson D, Lohmann C, et al. Cellular and nerve regeneration within a biosynthetic extracellular matrix for corneal transplantation. *Proc Natl Acad Sci U S A*. 2003;100(26):15346-15351. doi:10.1073/pnas.2536767100.
12. Maurice DM. The structure and transparency of the cornea. *J Physiol*. 1957;136(2):263-286. doi:10.1113/jphysiol.1957.sp005758.
13. Beales MP, Funderburgh JL, Jester JV, Hassell JR. Proteoglycan synthesis by bovine keratocytes and corneal fibroblasts: maintenance of the keratocyte phenotype in culture. Investigative ophthalmology & visual science. 1999 Jul 1;40(8):1658-63.
14. Robert L, Legeais JM, Robert AM, Renard G. Corneal collagens. *Pathol Biol (Paris)*. 2001;49(4):353-363. http://www.ncbi.nlm.nih.gov/pubmed/11428172. Accessed September 19, 2017.
15. Schultz GS, Wysocki A. Interactions between extracellular matrix and growth factors in wound healing. *Wound Repair Regen*. 2009;17(2):153-162. doi:10.1111/j.1524-475X.2009.00466.x.
16. Donohue DJ, Stoyanov BJ, McCally RL, Farrell RA. Numerical modeling of the cornea's lamellar structure and birefringence properties. *J Opt Soc Am A*. 1995;12(7):1425.

doi:10.1364/JOSAA.12.001425.

17. C Cintron; H Covington; C L Kublin. Morphogenesis of rabbit corneal stroma. *Invest Ophthalmol Vis Sci*. 1983;24(5):543-556. http://iovs.arvojournals.org.proxy.library.uu.nl/article.aspx?articleid=2176646. Accessed January 10, 2018.
18. Nucci P, Brancato R, Mets MB, Shevell SK. Normal Endothelial Cell Density Range in Childhood. *Arch Ophthalmol*. 1990;108(2):247. doi:10.1001/archopht.1990.01070040099039.
19. Tadashi Senoo; Nancy C. JoyceJoyce NC. Cell Cycle Kinetics in Corneal Endothelium from Old and Young Donors. *Invest Ophthalmol Vis Sci*. 2000;41(3):660-667. http://iovs.arvojournals.org.proxy.library.uu.nl/article.aspx?articleid=2199912. Accessed January 10, 2018.
20. Geroski DH, Matsuda M, Yee RW, Edelhauser HF. Pump Function of the Human Corneal Endothelium: Effects of Age and Cornea Guttata. *Ophthalmology*. 1985;92(6):759-763. doi:10.1016/S0161-6420(85)33973-8.
21. Pascolini D, Mariotti SP. Global estimates of visual impairment: 2010. *Br J Ophthalmol*. 2012;96(5):614-618. doi:10.1136/bjophthalmol-2011-300539.
22. He J, Bazan NG, Bazan HEP. Mapping the entire human corneal nerve architecture. *Exp Eye Res*. 2010;91(4):513-523. doi:10.1016/J.EXER.2010.07.007.
23. Leslie Paton. The trigeminal and its ocular lesions. *J Tissue Eng Regen Med*. 1926;10(6):305-342. doi:10.1002/term.2621.
24. Guthoff RF, Wienss H, Hahnel C, Wree A. Epithelial Innervation of Human Cornea. *Cornea*. 2005;24(5):608-613. doi:10.1097/01.ico.0000154384.05614.8f.
25. Shaheen BS, Bakir M, Jain S. Corneal nerves in health and disease. *Surv Ophthalmol*. 2014;59(3):263-285. doi:10.1016/j.survophthal.2013.09.002.
26. Madduri S, Papaloïzos M, Gander B. Synergistic effect of GDNF and NGF on axonal branching and elongation in vitro. *Neurosci Res*. 2009;65(1):88-97. doi:10.1016/J.NEURES.2009.06.003.
27. Lopatina T, Kalinina N, Karagyaur M, et al. Adipose-Derived Stem Cells Stimulate Regeneration of Peripheral Nerves: BDNF Secreted by These Cells Promotes Nerve Healing and Axon Growth De Novo. Egles C, ed. *PLoS One*. 2011;6(3):e17899. doi:10.1371/journal.pone.0017899.
28. Von Korff M, Dunn KM. Chronic pain reconsidered. *Pain*. 2008;138(2):267-276. doi:10.1016/J.PAIN.2007.12.010.
29. Beuerman RW, Schimmelpfennig B. Sensory denervation of the rabbit cornea affects epithelial properties. *Exp Neurol*. 1980;69(1):196-201. doi:10.1016/0014-4886(80)90154-5.
30. Nishida T, Chikama T-I, Sawa M, Miyata K, Matsui T, Shigeta K. Differential contributions of impaired corneal sensitivity and reduced tear secretion to corneal epithelial disorders. *Jpn J Ophthalmol*. 2012;56(1):20-25. doi:10.1007/s10384-011-0105-4.
31. Heigle Thomas J. M.D.; Pflugfelder SCMD. Aqueous Tear Production in Patients with Neurotrophic Kerati... : Cornea. *Cornea*. 1996;3.
33. Ghanem VC, Ghanem RC, de Oliveira R. Postoperative Pain After Corneal Collagen Cross-Linking. *Cornea*. 2013;32(1):20-24. doi:10.1097/ICO.0b013e31824d6fe3.

33. Andrea Cruzat; Deborah Witkin; Neda Baniasadi; Lixin Zheng; Joseph B. Ciolino; Ula V. Jurkunas; James Chodosh; Deborah Pavan-Langston; Reza Dana; Pedram Hamrah. Inflammation and the Nervous System: The Connection in the Cornea in Patients with Infectious Keratitis. *Investig Opthalmology Vis Sci*. 2011;52(8):5136. doi:10.1167/iovs.10-7048.
34. Hargus NJ, Patel MK. Voltage-gated Na channels in neuropathic pain. *Expert Opin Investig Drugs*. 2007;16(5):635-646. doi:10.1517/13543784.16.5.635.
35. Malik RA, Kallinikos P, Abbott CA, et al. Corneal confocal microscopy: a non-invasive surrogate of nerve fibre damage and repair in diabetic patients. *Diabetologia*. 2003;46(5):683-688. doi:10.1007/s00125-003-1086-8.
36. Tripathi BJ, Tripathi RC. Cytotoxic effects of benzalkonium chloride and chlorobutanol on human corneal epithelial cells in vitro. *Lens Eye Toxic Res*. 1989;6(3):395-403.
37. Geerling G, Daniels JT, Dart JK, Cree IA, Khaw PT. Toxicity of natural tear substitutes in a fully defined culture model of human corneal epithelial cells. *Invest Ophthalmol Vis Sci*. 2001;42(5):948-956.
38. Van Goethem F, Adriaens E, Alépée N, et al. Prevalidation of a new in vitro reconstituted human cornea model to assess the eye irritating potential of chemicals. *Toxicol Vitr*. 2006;20(1):1-17. doi:10.1016/J.TIV.2005.05.002.
39. Mohan RR, Possin DE, Mohan RR, Sinha S, Wilson SE. Development of genetically engineered tet HPV16-E6/E7 transduced human corneal epithelial clones having tight regulation of proliferation and normal differentiation. *Exp Eye Res*. 2003;77(4):395-407. doi:10.1016/S0014-4835(03)00175-1.
40. Reichl S, Bednarz J, Müller-Goymann CC. Human corneal equivalent as cell culture model for in vitro drug permeation studies. *Br J Ophthalmol*. 2004;88(4):560-565. doi:10.1136/BJO.2003.028225.
41. Chen Z, You J, Liu X, et al. Biomaterials for corneal bioengineering. *Biomed Mater*. 2018;13(3):32002. doi:10.1088/1748-605X/aa92d2.
42. Rönkkö S, Vellonen K-S, Järvinen K, Toropainen E, Urtti A. Human corneal cell culture models for drug toxicity studies. *Drug Deliv Transl Res*. 2016;6(6):660-675. doi:10.1007/s13346-016-0330-y.
43. Mimura T, Amano S, Yokoo S, et al. Tissue engineering of corneal stroma with rabbit fibroblast precursors and gelatin hydrogels. *Mol Vis*. 2008;14:1819-1828.
44. Watanabe R, Hayashi R, Kimura Y, et al. A novel gelatin hydrogel carrier sheet for corneal endothelial transplantation. *Tissue Eng Part A*. 2011;17(17-18):2213-2219. doi:10.1089/ten.TEA.2010.0568.
45. Ghasemi-Mobarakeh L, Prabhakaran MP, Morshed M, Nasr-Esfahani M-H, Ramakrishna S. Electrospun poly(ε-caprolactone)/gelatin nanofibrous scaffolds for nerve tissue engineering. *Biomaterials*. 2008;29(34):4532-4539. doi:10.1016/J.BIOMATERIALS.2008.08.007.
46. Loessner D, Meinert C, Kaemmerer E, et al. Functionalization, preparation and use of cell-laden gelatin methacryloyl–based hydrogels as modular tissue culture platforms. *Nat Protoc*. 2016. doi:10.1038/nprot.2016.037.

47. Gómez-Guillén MC, Giménez B, López-Caballero ME, Montero MP. Functional and bioactive properties of collagen and gelatin from alternative sources: A review. *Food Hydrocoll*. 2011;25(8):1813-1827. doi:10.1016/J.FOODHYD.2011.02.007.
48. Ghezzi CE, Rnjak-Kovacina J, Kaplan DL. Corneal Tissue Engineering: Recent Advances and Future Perspectives. *Tissue Eng Part B Rev*. 2015;21(3):278-287. doi:10.1089/ten.teb.2014.0397.
49. Gil ES, Mandal BB, Park S-H, Marchant JK, Omenetto FG, Kaplan DL. Helicoidal multi-lamellar features of RGD-functionalized silk biomaterials for corneal tissue engineering. *Biomaterials*. 2010;31(34):8953-8963. doi:10.1016/j.biomaterials.2010.08.017.
50. Lawrence BD, Pan Z, Rosenblatt MI. Silk film topography directs collective epithelial cell migration. *PLoS One*. 2012;7(11):e50190. doi:10.1371/journal.pone.0050190.
51. Bray LJ, George KA, Ainscough SL, Hutmacher DW, Chirila T V., Harkin DG. Human corneal epithelial equivalents constructed on Bombyx mori silk fibroin membranes. *Biomaterials*. 2011;32(22):5086-5091. doi:10.1016/j.biomaterials.2011.03.068.
52. Hu X, Shmelev K, Sun L, et al. Regulation of Silk Material Structure by Temperature-Controlled Water Vapor Annealing. *Biomacromolecules*. 2011;12(5):1686-1696. doi:10.1021/bm200062a.
53. Wang S, Ghezzi CE, Gomes R, Pollard RE, Funderburgh JL, Kaplan DL. In vitro 3D corneal tissue model with epithelium, stroma, and innervation. *Biomaterials*. 2017;112:1-9. doi:10.1016/J.BIOMATERIALS.2016.09.030.
54. Majumdar S, Guo Q, Garza-Madrid M, et al. Influence of collagen source on fibrillar architecture and properties of vitrified collagen membranes. *J Biomed Mater Res Part B Appl Biomater*. 2016;104(2):300-307. doi:10.1002/jbm.b.33381.
55. Borene ML, Barocas VH, Hubel A. Mechanical and cellular changes during compaction of a collagen-sponge-based corneal stromal equivalent. *Ann Biomed Eng*. 2004;32(2):274-283.
56. Calderón-Colón X, Xia Z, Breidenich JL, et al. Structure and properties of collagen vitrigel membranes for ocular repair and regeneration applications. *Biomaterials*. 2012;33(33):8286-8295. doi:10.1016/j.biomaterials.2012.07.062.
57. Zorn-Kruppa M, Tykhonova S, Belge G, Bednarz J, Diehl HA, Engelke M. A human corneal equivalent constructed from SV40-immortalised corneal cell lines. *Altern Lab Anim*. 2005;33(1):37-45.
58. Duan X, Sheardown H. Dendrimer crosslinked collagen as a corneal tissue engineering scaffold: Mechanical properties and corneal epithelial cell interactions. *Biomaterials*. 2006;27(26):4608-4617. doi:10.1016/J.BIOMATERIALS.2006.04.022.
59. Palchesko RN, Carrasquilla SD, Feinberg AW. Natural Biomaterials for Corneal Tissue Engineering, Repair, and Regeneration. *Adv Healthc Mater*. May 2018:1701434. doi:10.1002/adhm.201701434.
60. Koulikovska M, Rafat M, Petrovski G, et al. Enhanced regeneration of corneal tissue via a bioengineered collagen construct implanted by a nondisruptive surgical technique. *Tissue Eng Part A*. 2015;21(5-6):1116-1130. doi:10.1089/ten.TEA.2014.0562.
61. Cheng X, Gurkan UA, Dehen CJ, et al. An electrochemical fabrication process for the assembly of anisotropically oriented collagen bundles. *Biomaterials*. 2008;29(22):3278-3288.

doi:10.1016/j.biomaterials.2008.04.028.

62. Kishore V, Iyer R, Frandsen A, Nguyen T-U. *In vitro* characterization of electrochemically compacted collagen matrices for corneal applications. *Biomed Mater*. 2016;11(5):55008. doi:10.1088/1748-6041/11/5/055008.
63. Ahearne M, Wilson SL, Liu K-K, Rauz S, El Haj AJ, Yang Y. Influence of cell and collagen concentration on the cell–matrix mechanical relationship in a corneal stroma wound healing model. *Exp Eye Res*. 2010;91(5):584-591. doi:10.1016/J.EXER.2010.07.013.
64. Suuronen EJ, Nakamura M, Watsky MA, Stys PK, Müller LJ, Munger R, Shinozaki N, Griffith M. Innervated human corneal equivalents as in vitro models for nerve-target cell interactions. The FASEB journal. 2004 Jan;18(1):170-2.
65. Westerink RHS, Ewing AG. The PC12 cell as model for neurosecretion. *Acta Physiol (Oxf)*. 2008;192(2):273-285. doi:10.1111/j.1748-1716.2007.01805.x.
66. Leach JB, Brown XQ, Jacot JG, DiMilla PA, Wong JY. Neurite outgrowth and branching of PC12 cells on very soft substrates sharply decreases below a threshold of substrate rigidity. *J Neural Eng*. 2007;4(2):26-34. doi:10.1088/1741-2560/4/2/003.
67. Roeder BA, Kokini K, Sturgis JE, Robinson JP, Voytik-Harbin SL. Tensile Mechanical Properties of Three-Dimensional Type I Collagen Extracellular Matrices With Varied Microstructure. *J Biomech Eng*. 2002;124(2):214-222. doi:10.1115/1.1449904.
68. Sorkio A, Koch L, Koivusalo L, et al. Human stem cell based corneal tissue mimicking structures using laser-assisted 3D bioprinting and functional bioinks. *Biomaterials*. 2018;171:57-71. doi:10.1016/J.BIOMATERIALS.2018.04.034.
69. Isaacson A, Swioklo S, Connon CJ. 3D bioprinting of a corneal stroma equivalent. *Exp Eye Res*. 2018;173:188-193. doi:10.1016/J.EXER.2018.05.010.
70. Menei P, Pean JM, Nerrière-Daguin V, Jollivet C, Brachet P, Benoit JP. Intracerebral Implantation of NGF-Releasing Biodegradable Microspheres Protects Striatum against Excitotoxic Damage. *Exp Neurol*. 2000;161(1):259-272. doi:10.1006/EXNR.1999.7253.
71. Kirby GTS, White LJ, Steck R, et al. Microparticles for Sustained Growth Factor Delivery in the Regeneration of Critically-Sized Segmental Tibial Bone Defects. *Mater (Basel, Switzerland)*. 2016;9(4). doi:10.3390/ma9040259.
72. Lee CH, Shah B, Moioli EK, Mao JJ. CTGF directs fibroblast differentiation from human mesenchymal stem/stromal cells and defines connective tissue healing in a rodent injury model. *J Clin Invest*. 2010;120(9):3340-3349. doi:10.1172/JCI43230.
73. Hoch E, Hirth T, Tovar GEM, Borchers K. Chemical tailoring of gelatin to adjust its chemical and physical properties for functional bioprinting. *J Mater Chem B*. 2013;1(41):5675. doi:10.1039/c3tb20745e.
74. Chen Y-C, Lin R-Z, Qi H, et al. Functional Human Vascular Network Generated in Photocrosslinkable Gelatin Methacrylate Hydrogels. *Adv Funct Mater*. 2012;22(10):2027-2039. doi:10.1002/adfm.201101662.
75. Yue K, Trujillo-de Santiago G, Alvarez MM, Tamayol A, Annabi N, Khademhosseini A. Synthesis, properties, and biomedical applications of gelatin methacryloyl (GelMA) hydrogels.

*Biomaterials*. 2015;73:254-271. doi:10.1016/J.BIOMATERIALS.2015.08.045.

76. Kang L, Liu X, Yue Z, et al. Fabrication and In Vitro Characterization of Electrochemically Compacted Collagen/Sulfated Xylorhamnoglycuronan Matrix for Wound Healing Applications. *Polymers (Basel)*. 2018;10(4):415. doi:10.3390/polym10040415.
77. Younesi M, Islam A, Kishore V, Panit S, Akkus O. Fabrication of compositionally and topographically complex robust tissue forms by 3D-electrochemical compaction of collagen. *Biofabrication*. 2015;7(3):35001. doi:10.1088/1758-5090/7/3/035001.
78. Lopez-Garcia MDC, Beebe DJ, Crone WC. Young's modulus of collagen at slow displacement rates. *Biomed Mater Eng*. 2010;20(6):361-369. doi:10.3233/BME-2010-0649.
79. Kishore V, Iyer R, Frandsen A, Nguyen T-U. *In vitro* characterization of electrochemically compacted collagen matrices for corneal applications. *Biomed Mater*. 2016;11(5):55008. doi:10.1088/1748-6041/11/5/055008.
80. Hamilton KE, Pye DC. Young's Modulus in Normal Corneas and the Effect on Applanation Tonometry. *Optom Vis Sci*. 2008;85(6):445-450. doi:10.1097/OPX.0b013e3181783a70.
81. Hassell JR, Birk DE. The molecular basis of corneal transparency. *Exp Eye Res*. 2010;91(3):326-335. doi:10.1016/j.exer.2010.06.021.
82. Liu J, Lawrence BD, Liu A, Schwab IR, Oliveira LA, Rosenblatt MI. Silk Fibroin as a Biomaterial Substrate for Corneal Epithelial Cell Sheet Generation. *Investig Opthalmology Vis Sci*. 2012;53(7):4130. doi:10.1167/iovs.12-9876.
83. Mi S, Khutoryanskiy V V., Jones RR, Zhu X, Hamley IW, Connon CJ. Photochemical cross-linking of plastically compressed collagen gel produces an optimal scaffold for corneal tissue engineering. *J Biomed Mater Res Part A*. 2011;99A(1):1-8. doi:10.1002/jbm.a.33152.
84. Teng KK, Angelastro JM, Cunningham ME, Greene LA. Cultured PC12 cells: a model for neuronal function, differentiation, and survival. InCell biology 2006 Jan 1 (pp. 171-176)..
85. Tyson CA, Frazier JM. *Methods in Toxicology. Volume 1. Part A, In Vitro Biological Systems*.
86. Van Den Bulcke AI, Bogdanov B, De Rooze N, Schacht EH, Cornelissen M, Berghmans H. Structural and rheological properties of methacrylamide modified gelatin hydrogels. Biomacromolecules. 2000 Mar 14;1(1):31-8.
87. Lee BH, Lum N, Seow LY, Lim PQ, Tan LP. Synthesis and Characterization of Types A and B Gelatin Methacryloyl for Bioink Applications. *Mater (Basel, Switzerland)*. 2016;9(10). doi:10.3390/ma9100797.
88. Derakhshanfar S, Mbeleck R, Xu K, Zhang X, Zhong W, Xing M. 3D bioprinting for biomedical devices and tissue engineering: A review of recent trends and advances. *Bioact Mater*. 2018;3(2):144-156. doi:10.1016/J.BIOACTMAT.2017.11.008.
89. Zustiak SP, Pubill S, Ribeiro A, Leach JB. Hydrolytically degradable poly(ethylene glycol) hydrogel scaffolds as a cell delivery vehicle: characterization of PC12 cell response. *Biotechnol Prog*. 2013;29(5):1255-1264. doi:10.1002/btpr.1761.
90. Schuurman W, Levett PA, Pot MW, et al. Gelatin-Methacrylamide Hydrogels as Potential Biomaterials for Fabrication of Tissue-Engineered Cartilage Constructs. *Macromol Biosci*. 2013;13(5):551-561. doi:10.1002/mabi.201200471.

91. Müller LJ, Marfurt CF, Kruse F, Tervo TMT. Corneal nerves: structure, contents and function. *Exp Eye Res*. 2003;76(5):521-542. doi:10.1016/S0014-4835(03)00050-2.
92. Kapur TA, Shoichet MS. Immobilized concentration gradients of nerve growth factor guide neurite outgrowth. *J Biomed Mater Res*. 2004;68A(2):235-243. doi:10.1002/jbm.a.10168.
93. Makadia HK, Siegel SJ. Poly Lactic-co-Glycolic Acid (PLGA) as Biodegradable Controlled Drug Delivery Carrier. *Polymers (Basel)*. 2011;3(3):1377-1397. doi:10.3390/polym3031377.
94. Simón-Yarza T, Formiga FR, Tamayo E, Pelacho B, Prosper F, Blanco-Prieto MJ. PEGylated-PLGA microparticles containing VEGF for long term drug delivery. *Int J Pharm*. 2013;440(1):13-18. doi:10.1016/J.IJPHARM.2012.07.006.
95. Orth M, Kruse N, Braun B, et al. BMP-2-coated mineral coated microparticles improve bone repair in atrophic non-unions. *Eur Cells Mater*. 2017;33:1-12. doi:10.22203/eCM.v033a01.
96. Antman-Passig M, Levy S, Gartenberg C, Schori H, Shefi O. Mechanically Oriented 3D Collagen Hydrogel for Directing Neurite Growth. doi:10.1089/ten.tea.2016.0185.
97. Zeng W, Rong M, Hu X, et al. Incorporation of Chitosan Microspheres into Collagen-Chitosan Scaffolds for the Controlled Release of Nerve Growth Factor. Soncini M, ed. *PLoS One*. 2014;9(7):e101300. doi:10.1371/journal.pone.0101300.
98. Stevens L. Materials and processes for the biofabrication of peripheral nerve guides. *Univ Wollongong Thesis Collect 1954-2016*.
99. Gower NJD, Barry RJ, Edmunds MR, Titcomb LC, Denniston AK. Drug discovery in ophthalmology: past success, present challenges, and future opportunities. *BMC Ophthalmol*. 2016;16(1):11. doi:10.1186/s12886-016-0188-2.
100. Raymond A. Huml, Cadmus Rich, and Kamali Chance. Key Challenges to US Topical Ocular Drug Development. *Regul Focus*. 2009;14:47-52.
101. Short BG. Safety Evaluation of Ocular Drug Delivery Formulations: Techniques and Practical Considerations. *Toxicol Pathol*. 2008;36(1):49-62. doi:10.1177/0192623307310955.
102. Draize JH. Methods for the study of irritation and toxicity of substances applied topically to the skin and mucous membranes. J. Pharmacol. Exp. Ther.. 1944;82:377-90.
103. Davila JC, Rodriguez RJ, Melchert RB, Acosta D. PREDICTIVE VALUE OF IN VITRO MODEL SYSTEMS IN TOXICOLOGY. *Annu Rev Pharmacol Toxicol*. 1998;38(1):63-96. doi:10.1146/annurev.pharmtox.38.1.63.
104. Jester J., Li L, Molai A, Maurer J. Extent of initial corneal injury as a basis for alternative eye irritation tests. *Toxicol Vitr*. 2001;15(2):115-130. doi:10.1016/S0887-2333(00)00065-5.
105. Patel S V., Bachman LA, Hann CR, Bahler CK, Fautsch MP. Human Corneal Endothelial Cell Transplantation in a Human Ex Vivo Model. *Investig Opthalmology Vis Sci*. 2009;50(5):2123. doi:10.1167/iovs.08-2653.
106. Sharma R, Ahuja M, Kaur H. Thiolated pectin nanoparticles: Preparation, characterization and ex vivo corneal permeation study. *Carbohydr Polym*. 2012;87(2):1606-1610. doi:10.1016/J.CARBPOL.2011.09.065.
107. Mishima S, Kudo T. In vitro incubation of rabbit cornea. Investigative Ophthalmology & Visual Science. 1967 Aug 1;6(4):329-39.

108. Shafaie S, Hutter V, Cook MT, Brown MB, Chau DYS. In Vitro Cell Models for Ophthalmic Drug Development Applications. *Biores Open Access*. 2016;5(1):94-108. doi:10.1089/biores.2016.0008.

109. Y Minami; H Sugihara; S Oono. *Reconstruction of Cornea in Three-Dimensional Collagen Gel Matrix Culture.* Vol 34. C.V. Mosby Co; 1993.

110. Tegtmeyer S, Reichl S, Müller-Goymann CC. Cultivation and characterization of a bovine in vitro model of the cornea. *Pharmazie*. 2004;59(6):463-471.

111. Zieske JD, Mason VS, Wasson ME, et al. Basement Membrane Assembly and Differentiation of Cultured Corneal Cells: Importance of Culture Environment and Endothelial Cell Interaction. *Exp Cell Res*. 1994;214(2):621-633. doi:10.1006/EXCR.1994.1300.

112. Reichl S, Döhring S, Bednarz J, Müller-Goymann CC. Human cornea construct HCC—an alternative for in vitro permeation studies? A comparison with human donor corneas. *Eur J Pharm Biopharm*. 2005;60(2):305-308. doi:10.1016/J.EJPB.2004.09.016.

113. L J Müller; G F Vrensen; L Pels; B N Cardozo; B Willekens. *Architecture of Human Corneal Nerves.* Vol 38. C.V. Mosby Co; 1997.

114. A. Huhtala, L. Salminen HT and HU. *Corneal Models for the Toxicity Testing of Drugs and Drug Releasing Materials*. 1st ed. (N. Ashammakhi, ed.).; 2008.

115. Knowlton, S., Anand, S., Shah, T., & Tasoglu, S. (2018). Bioprinting for neural tissue engineering. *Trends in neurosciences*, *41*(1), 31-46.

116. Sharma, R., Smits, I. P., De La Vega, L., Lee, C., & Willerth, S. M. (2020). 3D bioprinting pluripotent stem cell derived neural tissues using a novel fibrin bioink containing drug releasing microspheres. *Frontiers in bioengineering and biotechnology*, *8*, 57.

# Review paper

## Advanced fabrication approaches to controlled delivery systems for epilepsy treatment

Gilles van Tienderen[1,2a], Marius Berthel[1,3a], Zhilian Yue[1], Mark Cook[1,4,5], Xiao Liu[1], Stephen Beirne[1], Gordon G. Wallace[1]

1 ARC Centre of Excellence for Electromaterials Science, Intelligent Polymer Research Institute, AIIM Facility, University of Wollongong, NSW 2522, Australia

2 Utrecht University, Utrecht, The Netherlands

3 Department for Functional Materials in Medicine and Dentistry, University Hospital Wuerzburg, Pleicherwall 2, 97070 Wurzburg, Germany.

4 Clinical Neurosciences, St. Vincent's Hospital, 5th Floor, Daly Wing, 35 Victoria Parade, Fitzroy, Victoria 3065, Australia

5 Department of Medicine, University of Melbourne, St. Vincent's Hospital, 35 Victoria Parade, Fitzroy, Victoria 3065, Australia

a These authors contributed equally to this work

ABSTRACT

Introduction: Epilepsy is a chronic brain disease characterized by unprovoked seizures, which can have severe consequences including loss of consciousness and death. Currently, 30% of epileptic patients do not receive adequate seizure alleviation from oral routes of medication, despite many new medications becoming available over the last 20 years. A range of mechanisms have been postulated to account for this, including peripheral metabolism of the agents, poor absorption, and difficulty traversing the blood-brain barrier. Over the last decade, local drug delivery to the focal area of the brain where the seizure originates has emerged as a potential alternative, and may be achieved through the fabrication of drug-loaded polymeric implants for controlled on-site delivery. The emergence of novel advanced fabrication techniques has led to potential avenues to further augment implant-based drug delivery systems, particularly for epilepsy treatment.

Areas covered: This review presents an overview of the latest advanced fabrication techniques for controlled drug delivery systems for refractory epilepsy treatment. Recent advances in the different techniques are highlighted and the limitations of the respective techniques are discussed.

Expert opinion: Advances in biofabrication technologies are expected to enable a new paradigm of local drug delivery systems through offering high versatility in controlling drug release profiles, personalized customization and multi-drug incorporation. Tackling some of the current issues with advanced fabrication methods, including adhering to GMP-standards and industrial scale-up, together with innovative solutions for complex designs will see to the maturation of these techniques and result in increased clinical research into implant-based epilepsy treatment.

# Other Supplementary Materials

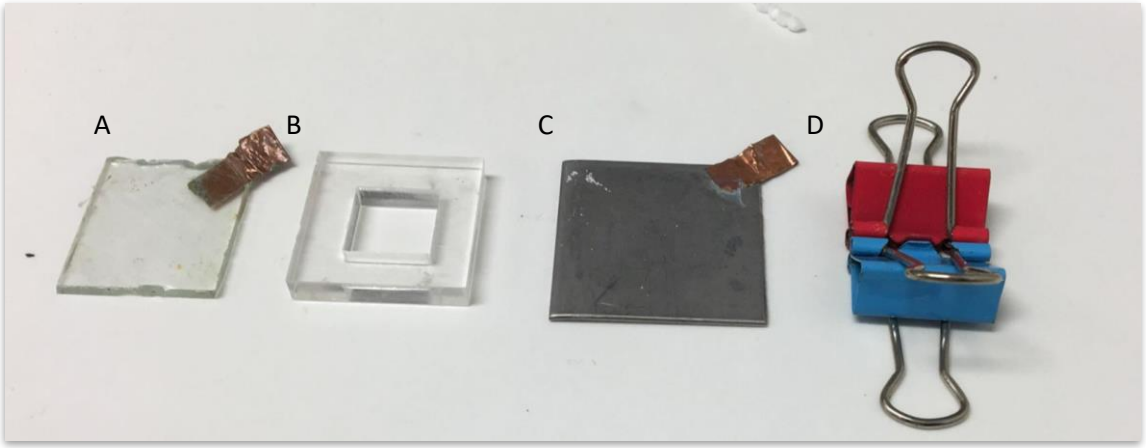


Supplemental figure 1: Complete set-up of the chamber used for electrocompaction of collagen. (A) ITO-coated glass, (B) non-conducive spacer (C) Stainless steel plate (D) Clamps

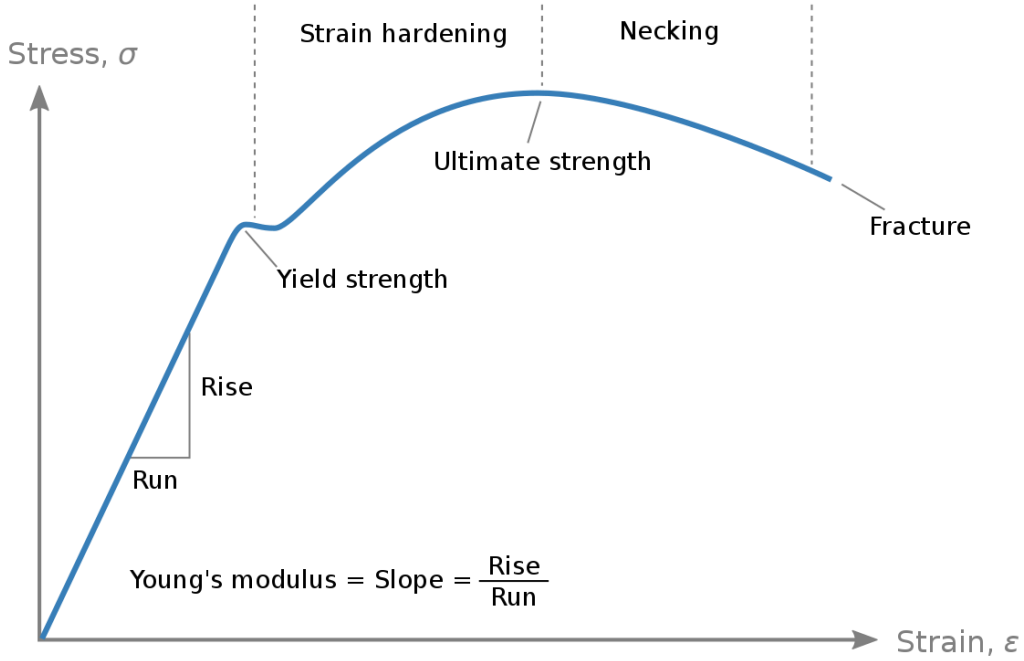


Supplemental figure 2: Example of a Stress strain curve conventionally obtained by tensile testing.

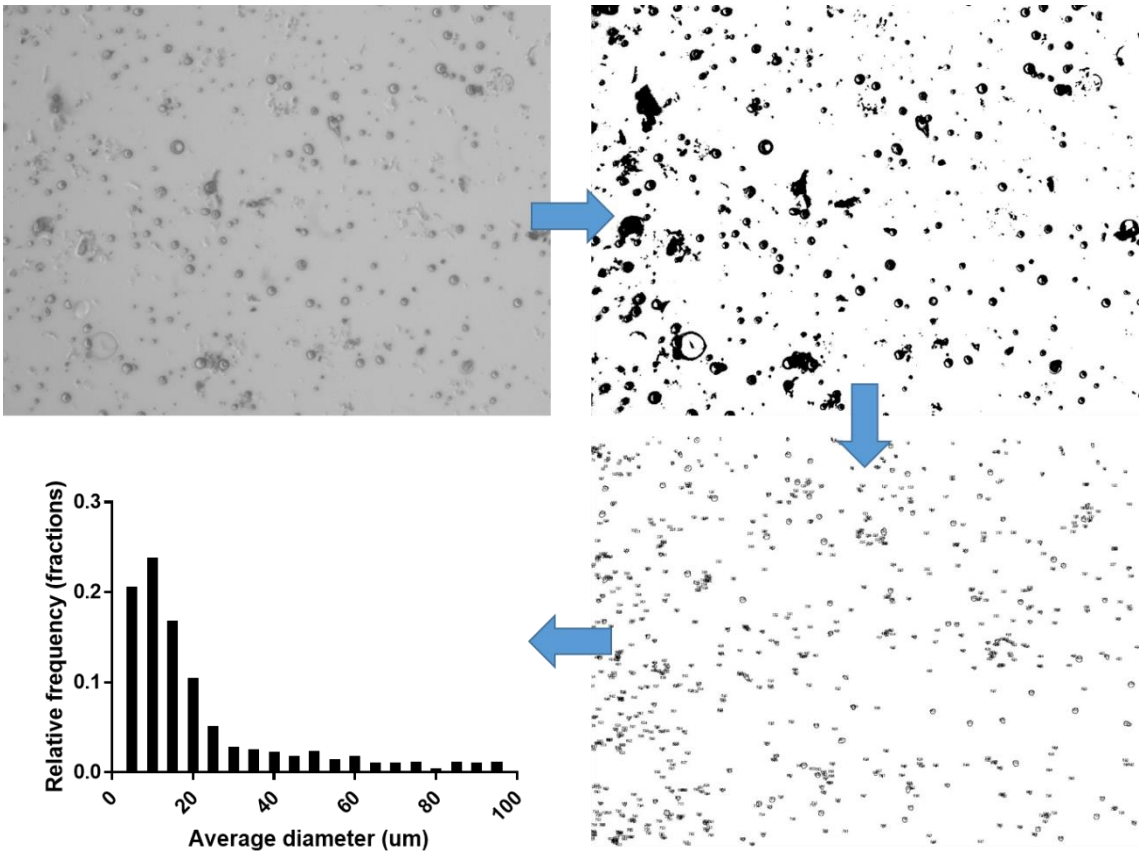


Supplemental figure 3: Sequential steps of microparticle size characterization. (Top left) Microscopic image in 16 bit image.; (Top right) Binarized image of microscopic image.; (Bottom right) Particle counting, removal of irregularities and evaluation of the diameter of the microparticles based on scaling of pixels .; (Bottom left) Example of histogram generated through this method of particle counting. ImageJ software was used for all steps.

\

Supplemental figure 4: schematic representation of full set-up of the proposed innervated corneal model.

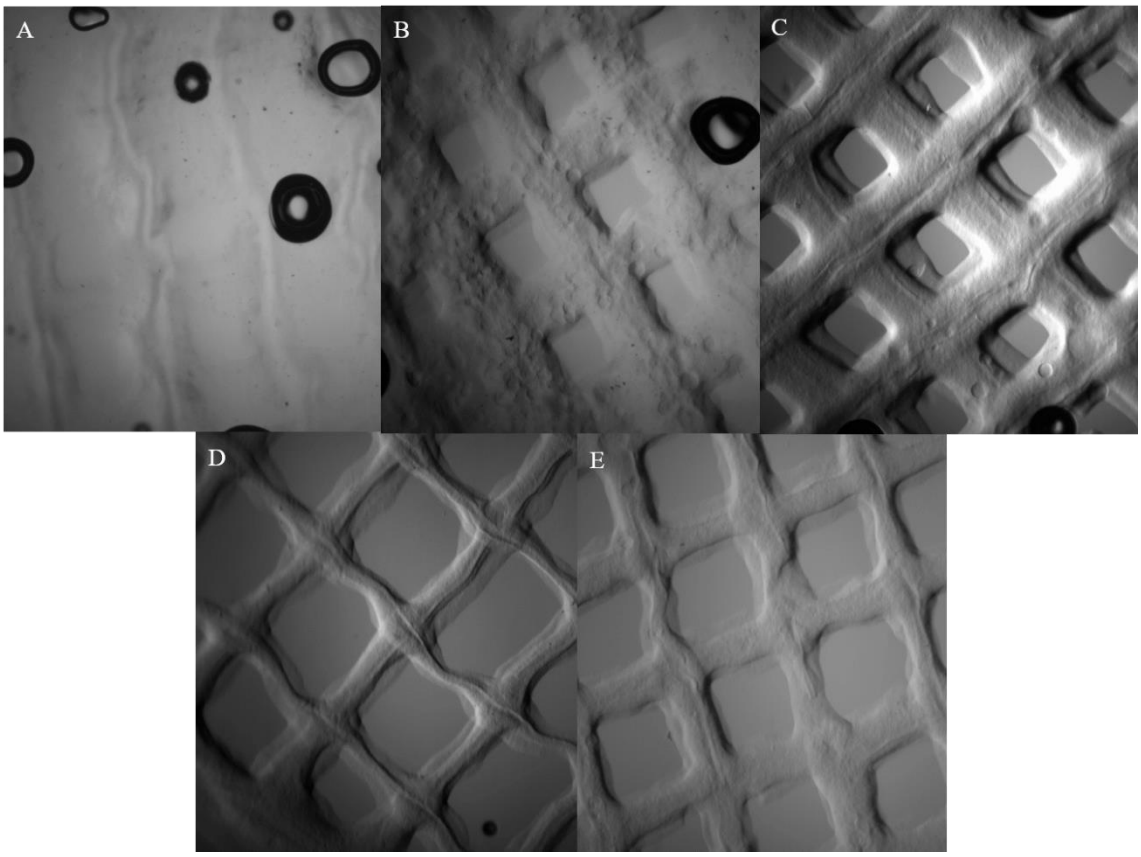


Supplemental figure 5: Optimalisation steps of printing parameters (Pressure, temperature, and speed) for 10% w/v GelMA with the Bioplotter. (A) 3.5 bar – 25C – 5 mm/s (B) 3.2 bar – 24C – 6 mm/s (C) 3.0 bar – 25C – 6 mm/s (D) 2.5 bar – 25C – 5 mm/s (E) 3.0 bar – 23C – 6 mm/s

Supplemental figure 6: Direct electrcompaction onto a preprinted PCL scaffold through assembling the chamber around the scaffold before injecting the collagen solution.

# Biofabrication double degree statement

According to the Memorandum of Agreement between: Queensland University of Technology, University of Wollongong, Julius-Maximilians-Universität Würzburg and Utrecht University, the Biofabrication Double degree master's program was started.

Students in the programme will be expected to obtain a Master's degree from one European and one Australian institution. The student initiates the Biofabrication Mobility Programme in a Master's degree at the home institution for two semesters (60 EC in Europe) over one year, prior to taking up enrolment in another Master's degree at the overseas participating institution, hereinafter referred to host institution, for a period of two semesters (60 EC in Europe) over one year.

Students shall enrol in a Master's degree at the home institution in accordance with the Biofabrication Mobility Programme specifications approved jointly by the institutions. Students will undertake a research project at the host institution in accordance with the project descriptions provided by each institution (supervisory and infrastructure capacity).

**The project undertaken at Utrecht University is currently involved in a pending patent application, and is therefore not attached as an additional appendix. However, it has successfully been submitted as part of the fulfillment of the Double Degree Masters of Biofabrication between UoW and University Utrecht.**